



Design and optimisation of a one-piece CFRP  
wheel for a Formula SAE vehicle

Giacomo Sammons  
C1262512

Supervisors: Rhys Pullin and Mark Eaton

April 2016

I hereby declare: That except where reference has been clearly made to work by others, all the work presented in this report is my own work; that it has not previously been submitted for assessment; and that I have not knowingly allowed any of it to be copied by another student.

I understand that deceiving or attempting to deceive examiners by passing off the work of another as my own is plagiarism. I also understand that plagiarising the work of another or knowingly allowing another student to plagiarise from my work is against the University regulations and that doing so will result in loss of marks and possible disciplinary proceedings against me.

Signed:

Date:

## Acknowledgements

I would like to express my gratitude to my supervisors, Dr. Mark Eaton and Dr. Rhys Pullin for the support and guidance they have given me. Their knowledge of and enthusiasm for the subject of fiber-reinforced composites was critical to the completion of this project and inspired me to further my knowledge in this field of Engineering. I would like to thank Garry Shipley for having been so kind and helpful during the manufacturing and curing of the CFRP components used in this project. Finally I would like to thank Cardiff Racing for having involved me so much in these years, where I learnt so much and inspired me to undertake this difficult project.

## Abstract

This dissertation deals with the design of a novel automotive wheel for use on a Formula SAE car built utilizing carbon fiber reinforced composites. The objective of this study is to investigate the advantages of employing a lighter wheel, design a new wheel suitable to the new material and propose a satisfactory manufacturing method. The wheel design will be developed through physical tensile testing and finite element analysis using Abaqus. Further weight reductions will be attempted by optimization of the carbon fiber orientation, stack order and variable ply count.

Physical testing was performed on carbon fiber-foam sandwich blocks to determine the number of plies required to captivate a metallic stud representing the wheel retention pins. Extensive Abaqus work was conducted to evaluate and control the orientation of composite skins using Tsai-Hill laminate failure criteria. Iterative simulations and modifications to the layup count and orientation were performed until the wheel achieved a factor of safety greater than 2.0.

A one-piece wheel utilizing a foam core was developed theoretically weighing  $747.4g$ , a potential weight reduction of  $6.61kg$  over the current aluminium wheel set and a 7-piece aluminium mould capable of manufacturing the proposed wheel was designed.

## Table of Contents

|   |    |
|---|----|
| ACKNOWLEDGEMENTS .....  | I  |
| ABSTRACT .....  | II |
| PREFACE .....   | IV |
| NOMENCLATURE.....   | IV |
| 1. INTRODUCTION.....  | 1  |
| 1.1 INTRODUCTION TO FORMULA SAE .....                             | 1  |
| 1.2 THE IMPORTANCE OF WEIGHT .....                                | 1  |
| 1.3 FEASIBILITY STUDY FOR THE USE OF CARBON FIBRE COMPOSITES..... | 3  |
| 1.4 LITERATURE REVIEW AND COMPETITOR DESIGNS .....                | 5  |
| 2. WHEEL SURFACE DESIGN .....                                     | 7  |
| 3. WHEEL OPERATING CASES .....                                    | 12 |
| 4. MANUFACTURING METHOD.....                                      | 18 |
| 5. PHYSICAL TESTING.....  | 22 |
| 5.1 DERIVATION OF LOAD CASE .....                                 | 22 |
| 5.2 DESIGN OF A TEST SETUP .....                                  | 23 |
| 5.3 CFRP-FOAM MICROSCOPE ANALYSIS.....                            | 27 |
| 5.4 SHEAR TESTING .....   | 29 |
| 5.4.1 Yield Strength.....   | 29 |
| 5.4.2 Cyclic testing.....   | 32 |
| 6. COMPUTATIONAL SIMULATION .....                                 | 35 |
| 6.1 CASE SETUP, BOUNDARY CONDITIONS AND LOAD DEFINITIONS.....     | 35 |
| 6.2 EVALUATION OF KEIZER WHEELS .....                             | 37 |
| 6.3 SIMULATION AND DEVELOPMENT OF CFRP WHEEL.....                 | 38 |
| 7. PROJECT DISCUSSION .....                                       | 45 |
| 8. PROJECT CONCLUSION .....                                       | 48 |
| 9. FURTHER AREAS OF STUDY .....                                   | 49 |
| 10. APPENDICES .....  | 51 |
| A. 2x2 TWILL CFRP DATA SHEET .....                                | 51 |
| B. ROHACELL RIGID FOAM DATASHEETS .....                           | 52 |
| C. CFRP-FOAM STUD TESTING SAMPLES NAMING AND CONSTRUCTION.....    | 53 |
| D. UNIDIRECTIONAL CFRP DATA SHEET .....                           | 53 |
| 11. REFERENCES .....  | 54 |

## Preface

### Nomenclature

| <b>Symbol</b> | <b>Description</b>               | <b>SI - Units</b>  |
|---------------|----------------------------------|--------------------|
| $P$           | Power                            | W                  |
| $t$           | Time                             | s                  |
| $m$           | Mass                             | kg                 |
| $I$           | Moment of inertia                | Kg m <sup>2</sup>  |
| $r$           | Radius                           | m                  |
| $a$           | Linear acceleration              | m s <sup>-2</sup>  |
| $\mu$         | Coefficient of friction          | -                  |
| $v$           | Velocity                         | m s <sup>-1</sup>  |
| $F$           | Force                            | N                  |
| $w$           | Vehicle track width              | m                  |
| $l$           | Vehicle wheelbase                | m                  |
| $CG$          | Centre of gravity                | -                  |
| $RF$          | Reaction Force                   | N                  |
| $P_{dyn}$     | Dynamic Pressure                 | Pa                 |
| $M$           | Moment                           | Nm                 |
| $\rho$        | Density                          | Kg m <sup>-3</sup> |
| $CLA$         | Unreferenced Coefficient of lift | -                  |

# 1. Introduction

## 1.1 Introduction to Formula SAE

Formula SAE is a student vehicle design competition run by the Society of Automotive Engineers since the late 1980's. Originally organized in the United States of America with a loose rulebook, it rapidly became popular around the world and several regional events were started. In Europe there are events run in Italy, Germany, Austria, Spain and the United Kingdom amongst others. Its popularity has increased to a global participation of over 300 teams, who involve undergraduate students in the design, manufacture, assembly and racing of a car.

The vehicle is based on a set of regulations, called the “Formula”, to which all cars must adhere during competition. The result is a small open-wheel car whose power ranges between 30 and 80kW and weight between 150 and 300kg.

In the early days of Formula SAE, teams opted for large displacement 600cc Supersport bike engines inside steel spaceframes. Thanks to advancements in material science and the more common availability of exotic materials like aluminium honeycomb and fiber reinforced composites teams have been able to design lighter cars, improving the vehicle's power-to-weight ratio. Some cars became sufficiently light to afford to mount a smaller, lighter and more compact twin or single-cylinder engine.

## 1.2 The importance of weight

The topic of weight reduction in motorsport has always been a critical one. The gains made available by reduction of mass span all aspects of vehicle performance: engines need to propel a smaller mass (reaching higher straight-line speeds and lower average fuel consumption), brakes need to absorb less energy, drivers are less fatigued in unassisted steering and the

structural components will suffer lower stress levels. In addition tyres are loaded less and thus produce a higher peak coefficient of friction (Edmondson, 2011) and are able to achieve higher cornering speeds.

The development of aerodynamic devices mounted on the cars to develop negative lift augmented the effect of weight change: given a certain load  $x$  generated at a speed  $v$  in a corner by a car weighing a mass  $m$  using tyres of coefficient of friction  $\mu$ , a car will be able to corner at a centripetal acceleration  $a$  as given in Equation 1:

$$a = \mu \cdot \frac{m \cdot g + x}{m} \quad (1)$$

Whilst this is a simplistic model, it can be appreciated that by a reduction of mass, the value of the fraction in (1) will grow in value as  $m$  is reduced. The effect is further increased by lift force's dependency on the square of  $v$ , meaning that being able to corner faster will generate more aerodynamic load and will allow to corner at higher centripetal forces. To give an example, a late 2000's Formula One car has a weight effect (perceived through progressive consumption of fuel) of 0.03s per lap per  $kg$ , meaning a  $33kg$  reduction in weight yields approximately an entire second of lap time difference (McLaren Racing Limited).

The intensity with which racing teams have chased these gains has raised several issues, mainly vehicle safety, driver health and cost. For this reason most modern racing series impose a minimum weight that ensures chassis are sufficiently strong, drivers are not underweight and teams can compete with differing budgets.

The Formula SAE rulebook is one of the few exceptions to this restriction. This was likely allowed to give freedom to students to push their designs and utilize complex materials like carbon fiber reinforced polymers and advanced analysis packages, which they are likely to work with once they leave academia and work in engineering offices. Thanks to the growing popularity of aerodynamic packages, the intensity with which teams attempt to lose weight on their cars has increased.

### **1.3 Feasibility study for the use of Carbon Fibre Composites**

Cardiff Racing, the Formula SAE team run by Cardiff University in Wales, has been competing since 2003 and is in the process of developing its first car with an aerodynamics package. Striving to improve performance and climb the world rankings, the Team has looked into the use of carbon fiber reinforced composites, which will be referred to “CFRP” in this report. Past successful projects include the design and manufacture of a CFRP front impact structure (Baker, 2014) that saved around  $1kg$  and the manufacturing of lighter front and rear wings (Di Marino, 2016). Following a trend that already exists in Formula SAE, this project will attempt to design a novel, lighter wheel utilizing CFRP. A further step in the weight reduction will be performed by means of optimisation of the number and orientation of plies used in the sections of CFRP by exploiting the material’s anisotropic behavior.

Due to the limited budget available to Cardiff Racing it is important to evaluate the performance benefit of expensive projects before they are initiated. As previously explained, weight reduction brings significant improvements in several aspects of vehicle dynamics. A weight reduction specifically on a wheel brings additional benefits of reduction of the mass of the unsprung portions of the car (areas that the suspension system cannot control) and reduction in rotating mass. The latter is very important both in straight-line and in cornering performance. During cornering, rotating masses tend to resist changes in axis of rotation, known as gyroscopic effect. Not only the gyroscopic effect resists change of yaw of the car, it also induces a moment (Stengel, [no date]) that will detrimentally roll the car away from the inside of the corner. The numerical evaluation of this effect is complex and beyond the scope of this project. The second advantage mentioned, straight-line speed, will be equally important but can be calculated more easily. In order to understand the advantage one can consider the total inertia of a wheel accelerating on a flat surface. Due to friction it must roll as well as translate, meaning it’s total inertia will be the sum of its linear inertia  $m$  and it’s

rotational inertia  $I$ . If the wheel's radius of gyration (radius at which all the mass can be assumed to be concentrated, the rotational equivalent of a centre of gravity) is known, we can quantify the equivalent inertia that the wheel has.

Cardiff's three-piece wheel, shown in Figure 3, weighs  $2.4\text{kg}$  and has a radius of gyration of  $101\text{mm}$ . Using the equations for equivalent inertia (Ohio State, 2016) and the tyre radius of  $203\text{mm}$ , Cardiff Racing's wheels weigh  $9.6\text{kg}$  and contribute to  $14.4\text{kg}$  of inertia, of which  $4.8\text{kg}$  from rotation. By assuming that there is no other rotating part on the car and using the 2015 car's weight of  $250\text{kg}$  (including driver), its total inertia will be  $254.8\text{kg}$ . If the mass of the wheel can be reduced by  $1\text{kg}$  each, the mass of the car will drop to

$246\text{kg}$ , but the inertia will drop further to  $248.8\text{kg}$ . The mass of the car has reduced by  $1.55\%$  but the inertia has dropped by  $2.35\%$ . This is particularly valuable in the portions of time when the car is under traction-limited conditions. Given a coefficient of friction  $\mu$  of 1.0, the original car will propel at, based on Equation 1:

$$1 \cdot g \cdot \frac{250}{254.8} = 9.625 \text{m s}^{-2}$$

Using the same calculation for the lighter-wheel car described above, the acceleration increases to  $9.699 \text{m s}^{-2}$ , or  $0.77\%$  more under traction limited conditions; in non-traction limited conditions it will accelerate  $2.35\%$  faster. Given these advantages it is clear to the author that there is a justifiable benefit to the developing of novel, lighter CFRP wheels.



*Figure 3 – Three-piece aluminium Keizer wheels used by Cardiff Racing at time of writing (2016)*

## 1.4 Literature review and Competitor designs

Before starting any work, it is important to perform a literature review of available research on the topic and evaluate the competitions' wheel designs. There are two prevalent designs when looking at CFRP wheels: Three-piece wheels using metallic wheel centres and CFRP rim halves and one-piece CFRP wheels. The latter is more difficult to achieve due to added cost and manufacturing complexity as highlighted by Uyttersprot (2015) and Giber (2010). Uyttersprot (2015) offers a very thorough investigation into most aspects of wheel design and compares different levels of integration of CFRP in his proposed wheel designs. Uyttersprot (2015) obtains a mass reduction of 30% for three-piece CFRP-aluminium wheels and 40% for one-piece CFRP wheels on a car with similar kerb weight and identical baseline aluminium wheel rims (manufactured by Keizer, weighing 2.4kg each), totaling -3kg. Ressa (2013), as part of the team's effort to switch to 10-inch wheels designs developed a significant number of solutions covering one-piece CFRP shell wheels, two-piece bonded CFRP shell wheels and others. The results are summarized and converted to SI units in Table 1.

*Table 1 – A. Ressa (2013) summarized results for different wheel designs*

| Wheel design  | Mass / kg | Deflection / ° |
|---|-----------|----------------|
| Original 13" OZ aluminium wheel                       | 3.21      | 0.036          |
| One-piece CFRP shell wheel                            | 0.783     | 0.21           |
| Two-piece bonded CFRP shells                          | 0.892     | 0.14           |
| CFRP inner rim / aluminium wheel centre and outer rim | 1.359     | 0.275          |
| CFRP inner and outer rim / aluminium wheel centre     | 0.898     | 0.28           |



Figure 1 – Extract CAD drawing from A. Ressa (2013) report on CFRP wheels, showing a one-piece CFRP wheel

While comparison is not possible between the baseline wheel used by Ressa (2013) and his proposed CFRP-based wheels due to different wheel diameter, it is interesting to compare these weights of the solutions found by him and the weight reduction that are obtained with his one-piece CFRP wheels, shown in Figure 1. If they were to replace the 10-inch Keizer wheels, the weight reduction for the car would be  $-6.4\text{kg}$  throughout the

car (all four wheels replaced with CFRP ones). Rohan (2015) investigated replacing of the aluminium wheel rim shells and by design of a CFRP-foam sandwich section was able to reduce the global deformation from  $0.653\text{mm}$  to  $0.271\text{mm}$ . The paper only details that the section was composed of 8 plies of CFRP of unknown weight but used a  $15\text{mm}$  rigid foam core.

Other teams were consulted for the design of their CFRP wheels at Formula SAE competitions but refused to share details of the construction of their wheels except their mass. TU Graz developed a 10-inch one-piece CFRP-foam wheel that weighs below  $0.9\text{kg}$ , as have AMZ Racing from ETH Zurich, whose wheels weigh  $0.85\text{kg}$  each (Racecar Engineering, 2014). The latter released an assembly video of the CAD model of their car in 2015 where it is possible to capture a view of the cross-section of their wheel, visible in Figure 2. Team Bath Racing were also queried about their CFRP wheel rims and quoted a weight reduction of  $600\text{g}$  per wheel (Racecar



Figure 2 – Frame from AMZ Racing's assembly video showing section view of their CFRP wheels (AMZFormulaStudent, 2016)

Engineering, 2014).

With the use of information found and the quoted performance improvements it was estimated that designing of CFRP rim halves would bring a weight reduction of around 600g and a full CFRP wheel would bring a weight reduction in the region of 1.2kg per wheel. In order to maximize performance via weight reduction it was decided that this project should focus on the design of one-piece CFRP wheels. In order to avoid the issue of large wheel deformation seen by Ressa (2013) in its CFRP shell one-piece wheel (Figure 1) a sandwich structure utilizing a rigid foam core was chosen, similar to Figure 2.

## 2. Wheel surface design

The geometrical features of a wheel affect the shape of the tyre and consequently its performance (Smith, 2004). It is critical to ensure a good match between rim width and tyre pressure is obtained to get a flat and even contact patch. Avon tyres suggest running the tyres on rims between 7.0” and 8”. A few widths on the modular three-piece Keizer wheels were tested on track via measurement of tread temperature and a decision to run 7.5” was made. The new CFRP wheel intends to be a direct replacement for the Keizer wheel, mimicking its tyre interface surfaces, wheel offset and mounting to the axle face, as it can be seen in Figures 4 and 5.

These wheels are designed such that the drums allow for a very large internal diameter in the inside of the wheel, claimed by Keizer to be 9.5”. This is great for fitting of components in the wheel such as large diameter brake discs and tall uprights, as well as reducing the amount of air held in the tyre. The latter is a very important parameter to tyre performance as when the tyre heats up, the air inside it heats up with it, expanding and changing the tyre pressure and swelling the tyre. A reduced quantity of gas in the tyre will cause a smaller volumetric change and retain a more consistent tyre shape throughout the tyre temperature range.

This design decision is good for performance but causes issues with fitting of the tyre. Most car wheels feature a profile portion called the ‘drop centre’. This depression, visible in Figure 4 between the two rim halves, is necessary for allowing sitting one side of the tyre bead such that the other side can slip over the rim edge. This needs to be close to either of the lips of the wheel as if it were too far, the angle at which the tyre would have to be would make it very difficult to perform the task. This proved to be the case with the Keizer wheel setup, with the drop notch being too far from the outer lip of the tyre and requiring strong metallic levers to be used with great force. As this is particularly undesirable for a CFRP wheel, the wheel profile will be reshaped to improve the fitting procedure. While the Keizer wheels feature 10 quasi-radial spokes, it was deemed to be too complex to layup small thin surfaces. A study on reduction of spokes was performed: A higher spoke count would imply the wheel deflected in similar ways as it revolved and a lower spoke count would simplify manufacturing and provide for thicker walled carbon, reducing the risk of buckling. A middle ground of three spokes was chosen due to its ease of manufacture.

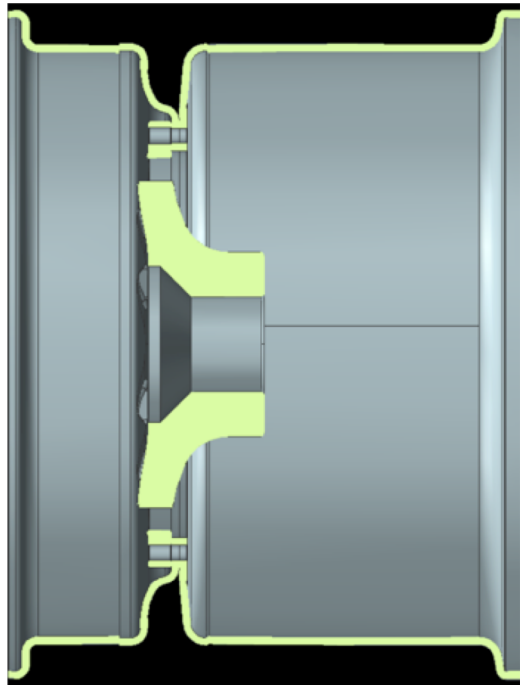


Figure 4 – Cardiff Racing Three-piece aluminium wheel CAD section view



Figure 5 – Cardiff Racing wheel top view

The tyre/wheel assembly undergoes deflection under cornering conditions. For this reason racing cars run static negative camber to ensure that when cornering the outside tyre, the more loaded one, has the largest contact patch thus the highest lateral force (Edmondson, 2011). The disadvantage in running higher static camber is that the tyre will have a reduced contact patch in straight-line conditions as it is angled to the track, and will lose longitudinal grip performance relative to a lower static camber setup. Some of this deflection comes from the wheel so it is important to design the wheel such that it will undergo as small deflection as possible under cornering.

This will be addressed by the use of a rigid closed-cell foam core in the wheel. Separating the CFRP laminates with a core will increase the section's moment of inertia and thus increase its stiffness. This core material was chosen over others due to its ability to be machined into complex shapes and its low resin absorption. It is desirable to minimize the latter effect to ensure the fibre volume fraction is maintained to the CFRP manufacturer's specification. Rohacell was chosen as the manufacturer of the foam thanks to their extensive line-up of foams of varying density and properties. The two types that will be used in the design of the CFRP wheel are HERO and RIMA. RIMA is marginally weaker but offers far lower resin adsorption, while HERO is available in high-density grade ( $200\text{kg m}^{-3}$ ). In order to reduce wheel deflection it was considered valuable to provide a stress path as straight as possible between the bore of the wheel and the wheel lip. This was not possible on the inner surface due to the current size and position of the components located inside the wheel (revolved assembly has a diameter of 9.25", or 235mm). On the outer surface this was performed by use of a smooth surface joining the wheel nut seat (which is at  $45^\circ$  from centerline) and the tyre lip.

A critical design criterion was to limit the curvature of the surfaces. Fabrics like that of carbon fiber have limited drapability (ability to lay a sheet without creases) on surfaces that exhibit

curvature in more than one direction. These surfaces are numerically evaluated by measurement of Gaussian curvature. This metric is the product of the radius of curvature in the two orthogonal principal directions. As explained by Aronsson (2005), this metric describes the amount of shear distortion in a sheet of material; In this case it would cause difficulty in following the curvature of the surface and cause distortion of fiber directions. For this reason an effort was made to reduce the size of surfaces that presented low Gaussian curvature. This was particularly relevant to the outer surface of the spokes, so the thickness of the spoke in side view was kept low. The radii of the fillets joining the spokes to the wheel drum were also kept to a small value due to a similar issue even though FEA (on NX Nastran) performed on a shell wheel made from isotropic material (aluminium) showed significant reductions in stress in these regions.

The resulting wheel surface design is shown in Figures 6, 7 and 8, the Gaussian curvature of the wheel in figure 9 and the isotropic FEA in figure 10.

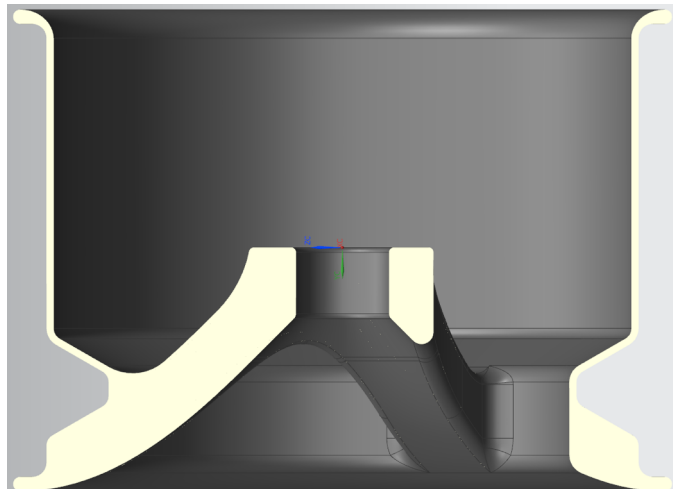


*Figure 6 – Section view of CFRP wheel*



*Figure 7 – Outboard view of CFRP wheel*

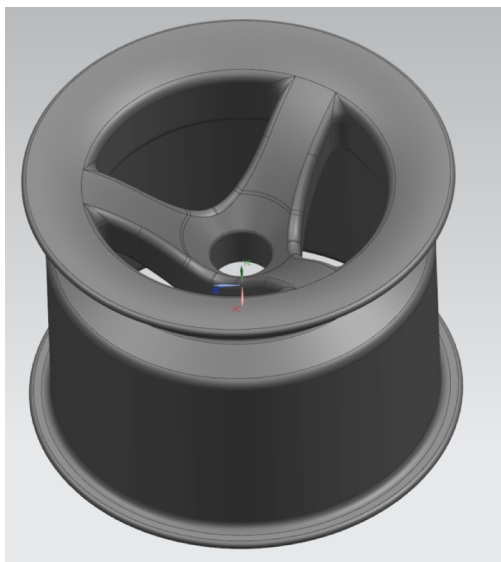


Figure 8 – Isometric view of CFRP wheel

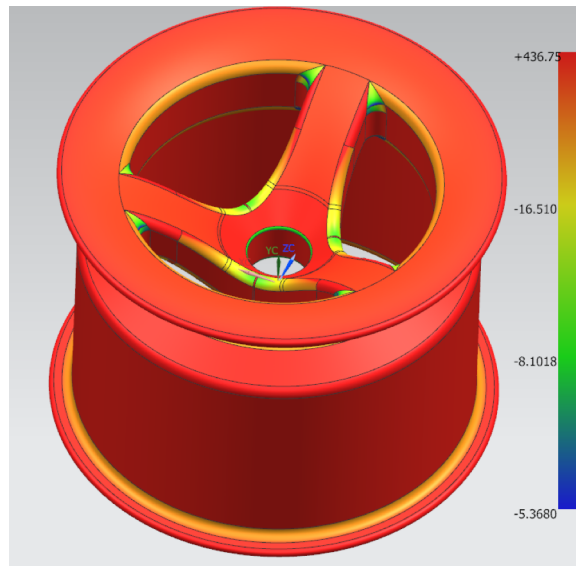


Figure 9 – Gaussian curvature analysis on CFRP wheel surface. Smaller numbers represent a surface more difficult to layup and are represented by cooler colors

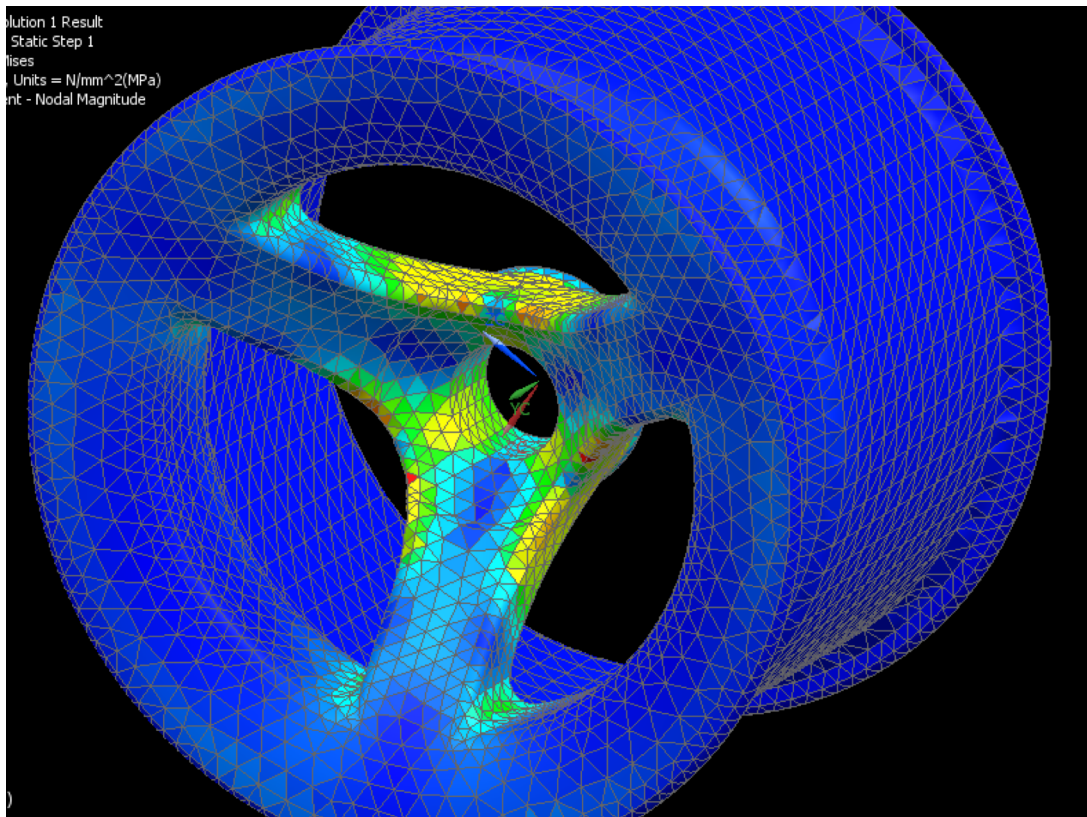


Figure 10 – NX Nastran FEA performed on a 2mm thick aluminium shell of the proposed wheel surface

### 3. Wheel Operating Cases

In order to define the load cases that the wheel will need to be developed around it is necessary to consider the vehicle dynamics of a typical automobile. For the first step of this analysis the model will be simplified such that tyres are point contacts and the axles are of equal width, such that the vehicle can be treated as a truss structure with pinned ends at the tyre contact points (Figure 11).

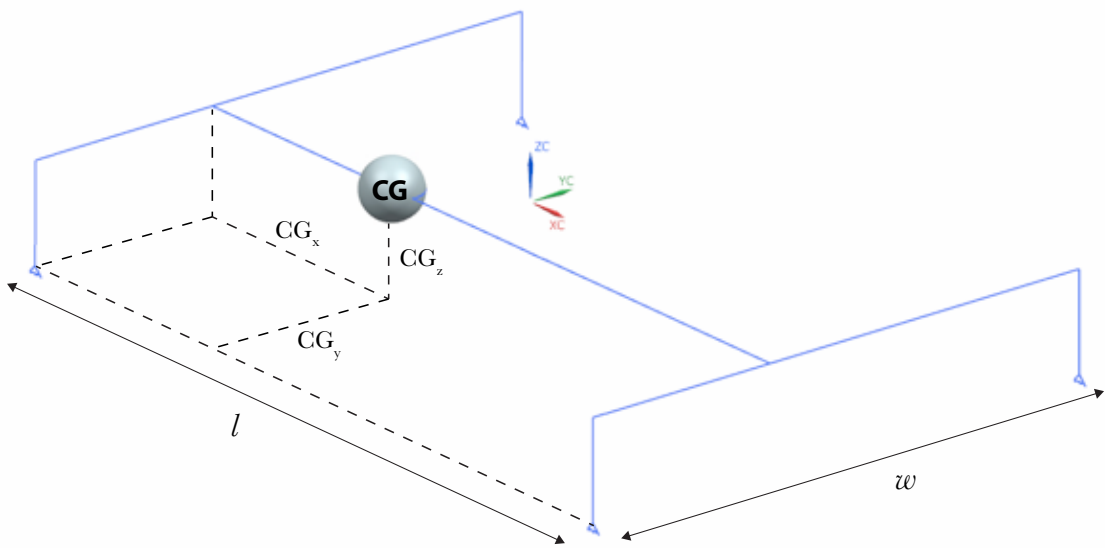


Figure 11 – Simplified model of automobile as trussed wireframe

The mass of the vehicle  $m$  can be considered to be concentrated at a point,  $CG$ , whose position is  $CG_x$  away from the front axle,  $CG_y$  from the rear axle and at a height of  $CG_z$  from the ground. Through equilibrium of forces and moments on the body it is possible to determine the vertical reaction forces  $RF_{FR}$ ,  $RF_{FL}$ ,  $RF_{RR}$ ,  $RF_{RL}$ , each corresponding to a corner of the car. For equilibrium of  $F_z$ ,  $M_x$  and  $M_y$  Equations 2, 3 and 4 can be setup:

$$\sum F_z = 0 = -m \cdot g + RF_{FR} + RF_{FL} + RF_{RR} + RF_{RL} \quad (2)$$

$$\sum M_x = 0 = (RF_{FR} + RF_{RR}) \cdot (w - CG_y) - (RF_{FL} + RF_{RL}) \cdot CG_y \quad (3)$$

$$\sum M_y = 0 = (RF_{FR} + RF_{FL}) \cdot CG_x - (RF_{RR} + RF_{RL}) \cdot (l - CG_x) \quad (4)$$

As there are more unknown variables than equations, it is not possible to determine the values of reaction force  $RF$  independently. The Equation 5 will represent the assumption that the ratio of  $RF$  between the wheels in each axle will be identical:

$$\frac{RF_{FR}}{RF_{FL}} = \frac{RF_{FR}}{RF_{FL}} \quad (5)$$

It is thus possible to derive the  $RF$  of each corner with Equations 2, 3, 4 and 5. Below the equation for  $RF_{FR}$  is then (Equation 6):

$$RF_{FR} = m \cdot g \cdot \frac{(w - CG_y)}{w} \cdot \frac{(CG_x)}{l} \quad (6)$$

Due to the recent trend of Formula SAE cars to sport wings in their design, it is important to take into consideration the vertical force generated by the aerodynamic devices often seen on Formula SAE cars in recent years. Utilizing Cardiff Racing's data from the past years' endurance events a value for maximum circuit speed  $v$  can be estimated at around  $25m/s$ . Utilizing this and an air density  $\rho$  of  $1.18 kg/m^3$  the dynamic pressure  $P_{dyn}$  can be calculated using Equation 7:

$$P_{dyn} = \frac{1}{2} \rho \cdot v^2 = 368.25 Pa \quad (7)$$

Cardiff Racing designed a wing package in 2016, which had an unreference coefficient of lift  $CLA$  of -1.047 whilst other teams like TU Munich have now achieved values of -3.00 (TU Fast team, 2015). These values were obtained in Computational Fluid Dynamics simulations and the divergence of results to the real world varies between 10% and 40% less lift than predicted (Buckingham, 2015). By accepting a limit-case lift coefficient  $CLA$  of -3.00, lift force  $F_z$  can be calculated as per Equation 8:

$$F_z = P_{dyn} \cdot CLA = -1104.75N \quad (8)$$

Cardiff Racing has been focusing on improving its lift coefficient so by using the limit-case coefficient it is possible to calculate the force applied through the wheel as the car travels in a straight line at  $25 m/s$ . Cardiff Racing has been developing cars that had a position of the CG

in the middle of the axles (left-to-right) and around the middle of the wheelbase (with driver seated) and have been having a mass  $m$  of around  $180\text{kg}$ . The aerodynamic package developed during the 2015 season weighed around  $10\text{kg}$  so for the design of this car an overall weight of  $200\text{kg}$  will be used. A driver of mass of  $80\text{kg}$  fully dressed will be considered in the calculation too, making for a total weight of  $280\text{kg}$ . Three load cases will be considered in the analysis: Cornering, braking and mixed cornering-braking. It was during a load similar to that of the latter case that caused a fatigued axle to fail in 2015 during FS Italy event (Cardiff Racing, 2015) so it can be assumed that this will be the most demanding case. Braking was chosen over acceleration as reaching the limit of traction at high speed, the point of highest vertical load due to negative lift, would be far beyond the power levels obtained by Cardiff Racing's current engine. The centre of gravity was measured both as part of this project at  $323\text{mm}$  from the ground and by the suspension team at  $316\text{mm}$  so for the sake of this analysis it will be set at  $320\text{mm}$ . Thus, when braking at an acceleration  $a_x$  a moment will be generated by the  $CG$  that will cause a weight transfer to the front axle. This can be calculated equilibrium Equations for moment  $M_y$  with reference to the rear contact point using Equations 9 and 10.

$$\sum M_y = 0 = a_x \cdot CG_z - (\Delta RF_{FL} + \Delta RF_{FR}) \cdot l \quad (9)$$

$$(\Delta RF_{FL} + \Delta RF_{FR}) = \frac{a_x \cdot CG_z}{l} \quad (10)$$

By using the assumption that the left suspension is symmetrical to the right suspension geometry and spring rate the load transfer to the right and left corner will be equal. Longitudinal acceleration  $a_x$  can also be replaced by vertical load multiplied by coefficient of friction  $\mu$  (Equation 11):

$$\Delta RF_{FR} = \frac{m \cdot g \cdot \mu \cdot CG_z}{2l} \quad (11)$$

When looking at the cornering case, a similar equation to that expressed in (Equation 9), with reference to the left side of the car, can be used to describe the lateral load transfer (Equation 12):

$$\sum M_x = 0 = a_y \cdot CG_z - (\Delta RF_{RR} + \Delta RF_{FR}) \cdot w \quad (12)$$

Because the suspension geometry and spring rate is not identical front to rear, the roll resistance of the front axle may differ from that of the rear, thus causing a different load change to the front right corner to that of the rear right. This difference may be exacerbated by the use of an anti-roll bar, which effectively increases the roll resistance and the portion of the load transfer to the front right corner. This means that it is possible that the front axle performs all the roll resistance, such as when running only a heave spring at the rear. Thus the load transfer to the front right corner, when cornering left, will be equal to  $\Delta RF_{FR}$  as shown in Equation 13:

$$\Delta RF_{FR} = \frac{m \cdot g \cdot \mu \cdot CG_z}{w} \quad (13)$$

It is possible to derive an estimate for  $\mu$  by looking at the steady state cornering velocity. This can be captured during the skid pad dynamic event (Figure 12). This consists of a figure of eight with an inner diameter of 15.25m. The event measures the time taken by the car to perform an entire lap of each circle and averages them.

### FSAE SKIDPAD LAYOUT

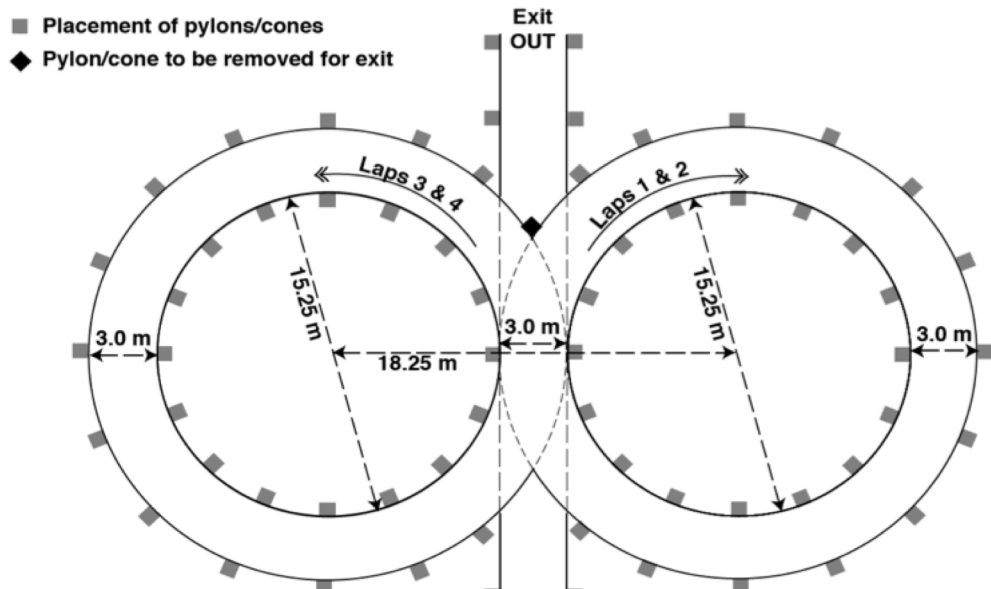


*Figure 12 – FSAE Skid Pad layout and dimensions*

Cardiff Racing had a best elapsed time of 5.2s without aerodynamic devices mounted with a car whose width was 1150mm. Assuming that the car was maintaining an average distance of 200mm from the inner circle (based on an average driver's accuracy from observations), the CG of the car was turning at a radius of half the inner circle diameter plus half the width of the car plus the gap between car and cones, or 8.4m. Using the equation of centripetal acceleration, it can be calculated using Equation 14 that:

$$a_y = \omega^2 r = \left(\frac{2\pi}{t}\right)^2 r = 12.25 m \cdot s^{-2} \quad (14)$$

This equates to a coefficient of friction  $\mu$  of 1.25. Taking into account the fact that the tyres are not at operating temperature and the event occurs on medium quality tarmac, a value of  $\mu$  of 1.5 will be used for the load cases.

For the mixed cornering it is important to take into consideration the traction circle of a tyre, a simplified model for a tyre's grip in the  $x$ - $y$  plane (Figure 13).

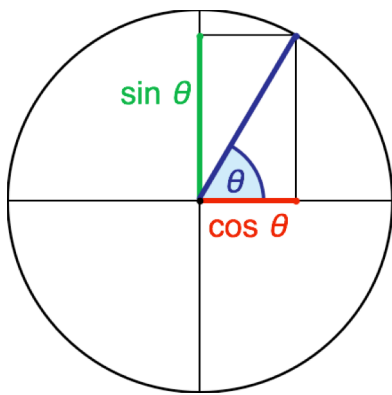


Figure 13 – Simplified tyre traction circle

By describing the direction of the load coplanar with the track as an angle  $\theta$  and identifying the length of the vector in the traction circle as  $mgu$ , Equations 11 and 13 can be expressed as sine and cosine functions of load transfer and used to describe the total load transfer to the front right corner:

$$\Delta RF_{FR} = \frac{m \cdot g \cdot \mu \cdot CG_z \cdot \sin(\theta)}{2l} + \frac{m \cdot g \cdot \mu \cdot CG_z \cdot \cos(\theta)}{w} \quad (15)$$

This equation can be plotted using Cardiff Racing's car wheelbase of 1550mm and track width of 1150mm to give a  $RF_{FR}$  to  $\theta$  plot (Figure 14):

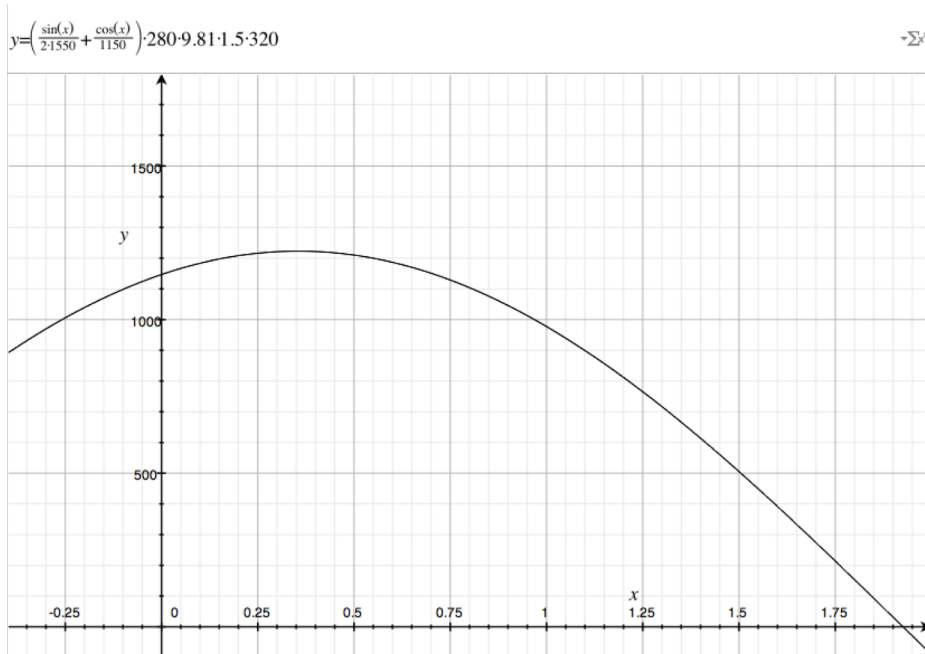


Figure 14 – Plot of Front right corner load to changes in theta

This can be differentiated and the peak vertical load derived. The simplified derivative through which the peak angle  $20.35^\circ$  can be calculated using Equation 16:

$$\frac{dRF_{FR}}{d\theta} = \frac{23\cos(\theta) - 62\sin(\theta)}{71300} \quad (16)$$

By using Equations 15 and 8 and the using the angles of  $0^\circ$  (pure cornering),  $90^\circ$  (pure braking) and the max  $RF_{FR}$  angle  $20.35^\circ$  (mixed braking-cornering), a table for the forces  $F_x$ ,  $F_y$ ,  $F_z$  in each load case can be populated (Table 2).

*Table 2 – Forces generated at Front right tyre contact patch at load-case angles*

| Tyre traction angle ( $\theta$ ) | $0^\circ$ | $90^\circ$ | $20.35^\circ$ |
|----------------------------------|-----------|------------|---------------|
| Normal Force ( $F_x$ ) / N       | 2937      | 2200       | 3013          |
| Longitudinal Force ( $F_y$ ) / N | 0         | 3324       | 1572          |
| Lateral Force ( $F_z$ ) / N      | 4405      | 0          | 4238          |

## 4. Manufacturing Method

In the process of designing the proposed CFRP wheel manufacturability was taken into account. This included the design of the moulds that will support the wheel during the curing process. Cardiff Racing has access to the University's autoclave oven, which allows curing at high temperatures under pressure with the part under vacuum. This reduces the options of a mould material to tooling board and aluminium. Aluminium was preferred over tooling board, as it doesn't degrade over time by cracking and chipping, as well as better matching the expansion ratio of CFRP (Engineering Toolbox, 2015) and being stronger. In order to ensure that the autoclave pressure compressed all the part it was necessary to consider which surfaces to bag and which to back on a mould. If a section is backed by two moulds it may not receive sufficient pressure and might develop air pockets which compromise the strength of the carbon (Marques et al, 2007), while if it is bagged on both sides it can warp and exceed dimensional tolerance. The tyre inner lip must also be smooth to ensure proper sealing of the

tyre. Figures 15, 16 show the rough surface that is generated on the bagged side due to the presence of a breather cloth and creases.



*Figure 15 – Surface roughness of cured CFRP flat sheet, breather cloth side*



*Figure 16 – Surface roughness on CFRP rim half from previous experiments*

With this consideration in mind it was deemed necessary to utilize an external hoop mould such that the surface finish was of sufficient smoothness to seal the tyre against the inner lip. This left the decision to either mould the inner face of the spokes or the outer face. By observing Figure 17 again it is possible to notice how the best surface to back with a mould is

the outer face. The inside of the hoop, the back and sides of the spokes will be bagged, leaving the only portion of the wheel not sandwiched between a bag and a mould that of the outer lip of a spoke section.

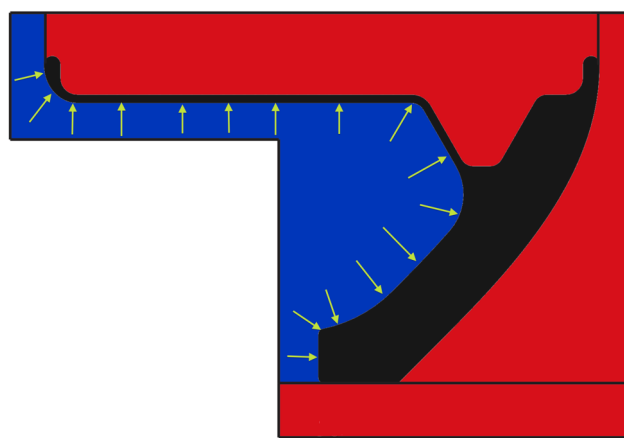


*Figure 17 – CFRP cross-section view of mould/bag split proposal, showing the wheel section in black, mould portions in red and bagged regions in blue. Arrows representing autoclave pressure*

curing is complete. The outer face mould will need to be manufactured from billet using a 3-

As it can be seen from Figure 18, the hoop mould was split into three parts to allow extraction of the part when

axis CNC machine whilst the split hoops may either be made from billets or from quasi-exact aluminium casts, to reduce machining cost. In either case, to ensure a step-free homogeneous surface the three parts will have the mating faces machined flat at 120 degrees, fastened together with bolts and then, once bolted together, turned on a numerical control lathe that will draw the internal profile. The three pieces will finally mate with the outer mould using fasteners. Tight tolerance holes for alignment pins will also be drilled on the external mould parts mating faces to facilitate alignment when reassembling the mould.

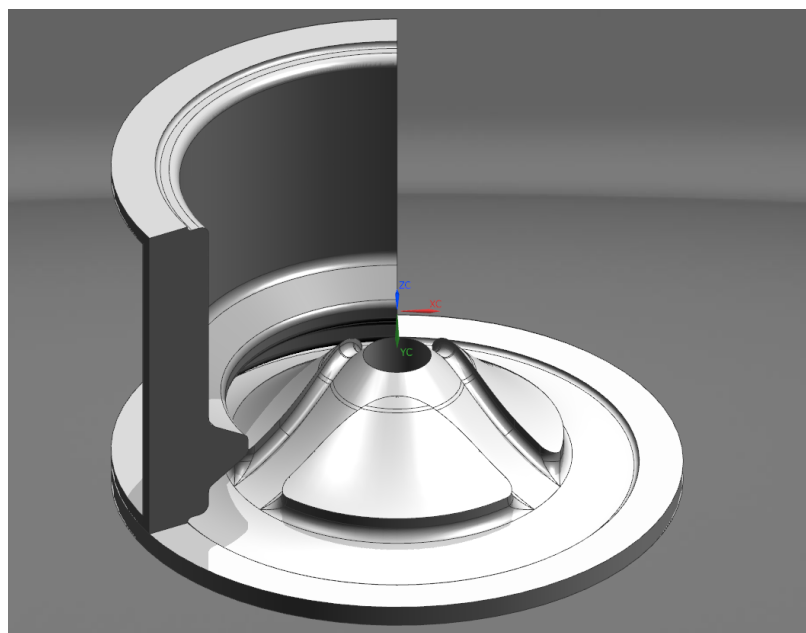


*Figure 18 – CFRP wheel external mould design*

A particularly difficult part to cure will be the straight bore of the wheel. As it will most certainly be impossible to extract a component with zero draft from the cured bore of the wheel, it is necessary to make a multi-piece aluminium assembly which can both generate sufficient pressure on the bore carbon plies and be able to be extracted. A solution was found by designing a three-piece insert, which has two arc segments and a wedge-type insert that will push the segments on the walls.

An additional complication that occurs in porting the geometrical features from the aluminium wheels is the retention system. This, visible in Figure 19, is composed of eight 8.5mm aluminium studs fitted inside drilled holes in the wheel centre. There are several

solutions to this application such as using an aluminium body at the wheel interface, but this creates the issue of joining back to the carbon. The best solution, although the least predictable, was deemed to be that of drilling the carbon fiber skin directly and bonding in the drilled holes the aluminium studs. As drilling CFRP causes the formation of interrupted fibres, standard composite theory is no longer valid. For this reason it was decided to identify the thickness of the CFRP required on the wheel mounting face via mechanical testing.



*Figure 19 – Cardiff Racing wheel-axle interface on aluminium wheel*

## 5. Physical Testing

### 5.1 Derivation of load case

Due to the limited supply of CFRP material, it was not possible to manufacture large components so only the drilled carbon on the wheel-mounting interface with the axle was tested. A torque is applied to an axle of a wheel when braking or accelerating. This torque is transferred to the wheel via the aluminium studs and to the tyre. This axle torque  $T$  is effectively applying a shear force  $F$  on the pins that will be equivalent to the torque over the radial distance of the pins to the centre of the axle. By utilizing the radial distance of the studs on the axles, equal to 28mm, and assuming that the studs share equal load so it is possible to derive the shear force shared by the each stud using Equation 17:

$$F = \frac{M}{8r} \quad (17)$$

By using the longitudinal force  $F_x$  generated by the front right wheel and using the diameter of 16" of the Avon tyres used on the Formula SAE car, the torque generated at the axle can be calculated as in Equation 18:

$$M = F_x \cdot r = 675Nm \quad (18)$$

Using Equation 17 and the resultant torque from Equation 18, the shear force to which each stud is stressed can be calculated. The equation assumes that the holes are drilled on the wheel and the axle with perfect tolerance and thus share the shear force equally (Equation 19).

$$F = \frac{M}{8r} = 3013N \quad (19)$$

## 5.2 Design of a test setup

In order to test the shear strength of a pin captivated in a carbon-foam wheel it is necessary to replicate the load path that would be seen by the wheel. The stud must be loaded in pure shear by applying tension in the plane of the wheel-axle mating surface. This is similar to test setups where bonding shear failure is measured on a single-lap joint, where spacers are placed each end to ensure no bending force is applied to the joint (Davis) such as it can be seen in Figure 20. In order to mimic the stress path that would be seen on the CFRP wheel, the carbon-foam sample was held by the sides orthogonal to the mounting face. These faces would be equivalent to the bore and outer diameter of the wheel, as it can be seen in the test setup in Figure 21 and the detail view of the CFRP wheel in Figure 22. To ensure no moments are applied at the ends during tensile testing spherical rod ends have been employed.

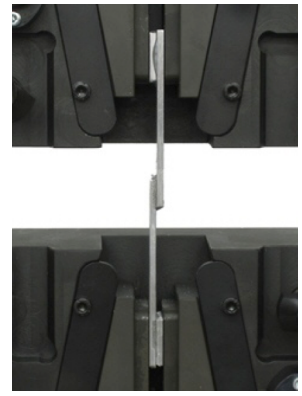


Figure 20 – Typical adhesive lap-shear joint test using spacers at the clamps

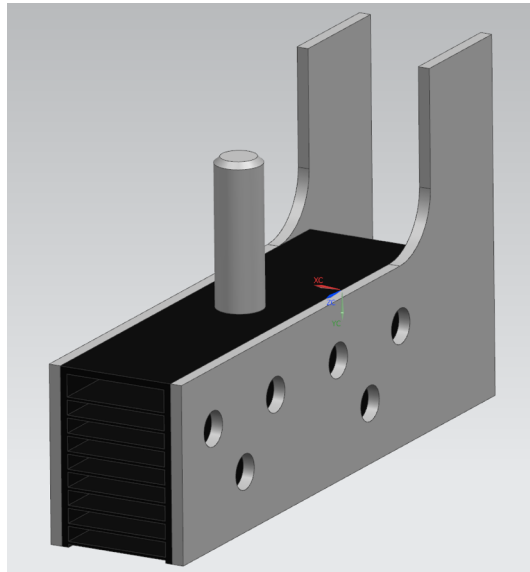


Figure 21 – CAD illustration of CFRP-foam tensile test sample mounting layout

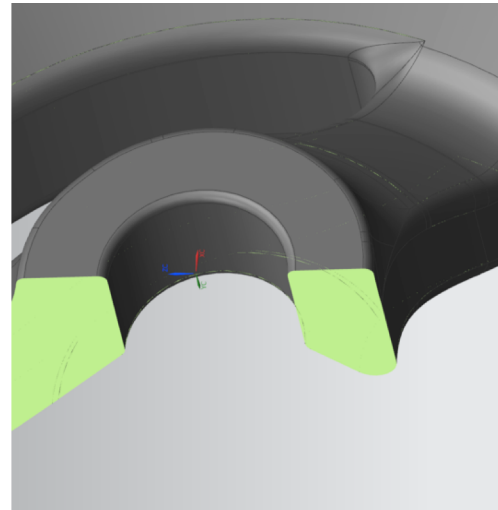


Figure 22 – CAD section view of wheel mounting face

In order to use one on the sample side, 2mm thick steel plates are bonded each side of the sample and are joined with fasteners to a metallic block that carries the rod end. A similar method of mounting the spherical rod is employed on the axle side, where a one-piece aluminium device retains the pin and stresses it in pure shear. A schematic view of the setup can be seen in Figure 23 as well as an image of the setup ready to be mounted on the tensile machine in Figure 24.

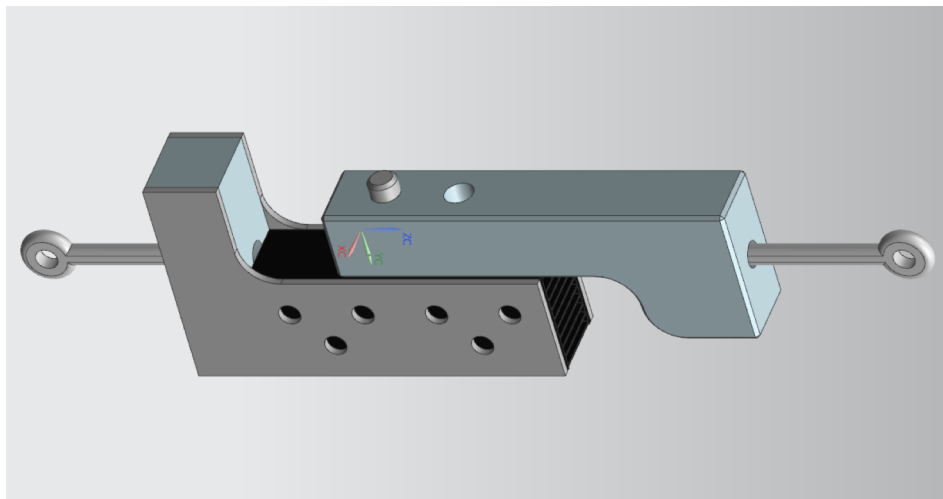


Figure 23 – CAD illustration of the complete stud testing assembly

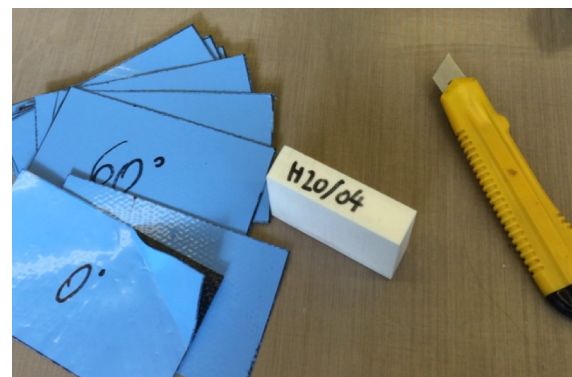


Figure 24 – Image of stud test setup before tensile experimentation

The carbon-foam samples were manufactured by cutting a large block of rigid foam into short blocks of a thickness of 18mm, slightly smaller than the wall thickness of the CFRP wheel bore inner to outer diameter difference to take into account the gain in thickness due to the

carbon layup. Given the CFRP wheel's three spoke design it was assumed that the plies from the spokes would extend to the axle face, thus coming at an angle of  $120^\circ$  to each other. The layups that would be tested would then be composed of ply stacks of  $0^\circ/30^\circ/60^\circ$  or symmetrical equivalents. An approximation was made that a wall thickness of at least  $2mm$  would be necessary to retain the stud with sufficient stiffness. For this reason two different layups were used,  $[0/30/60/60/30/0]_2$  and  $[0/30/60/60/30/0]_3$ , equal to a total number of plies of 12 and 18. Three different rigid foam cores were tested in conjunction with the two different layups: HERO 110, RIMA 110 and HERO 200. HERO is a high strength foam whilst RIMA is a low resin-adsorption one. The numbers represent the density of the foam, expressed in  $kg\ m^{-3}$ . The data for the CFRP is available in Appendix A and the data for Rohacell HERO and RIMA in Appendix B. Given a shortage of RIMA 110 and a similarity in property to that of HERO 110, only the two types of HERO will be tested on the 18-ply layup. A total of three samples for each combination of foam-carbon were manufactured, in order to be able to validate the consistency of the results. After performing a test to validate the cure cycle on a small batch of 8-ply CFRP-foam, a 1-hour cure cycle at a pressure of 400kPa with the part under vacuum was accepted for the main cure cycle of the test samples. The samples were labeled by marking them with a permanent marker before layup and ply stacks prepared, as is shown in Figure 25.

Once the layup was complete, the excess carbon was trimmed from the edges, as seen in Figure 26 in order to avoid bridging and formation of epoxy pockets, an issue that was noted during the test cure cycle and visible in Figure 27. Once all the foam blocks were laid with CFRP sheets



*Figure 25 – HERO 200 foam block ready for CFRP layup*

according to the intended layup, they were laid vertical on a PTFE table, covered with a release film and a breather and vacuumed. The process of vacuuming proved particularly difficult due to the large size of the bag and high number of pleats that were necessary to ensure there was enough excess bag to follow the contours of each sample. The bagged and vacuumed samples ready for curing are visible in

Figure 28. A list with the naming of each sample from

the second batch, their ply count and foam core is available in Appendix C.



Figure 26 – Untrimmed (right) and trimmed (left) CFRP plies on an 18-ply sample

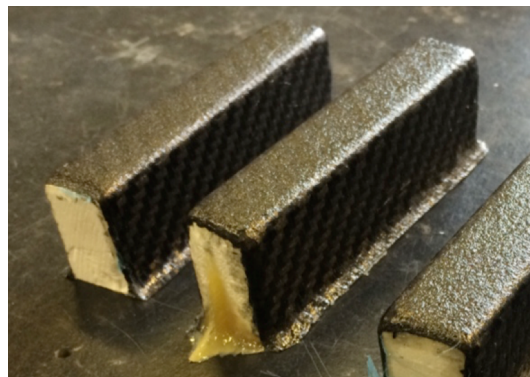


Figure 27 – First batch of CFRP samples, 8-ply, showing bridging of CFRP and epoxy pocket



Figure 28 – Samples bagged and vacuumed ready for curing in the autoclave.

### 5.3 CFRP-Foam Microscope Analysis

Due to concerns to damage to the plies due to the drilling of the holes for the studs, the samples used for testing of the cure cycle were drilled using high-speed steel drill bits in stages, using first a  $2.5\text{mm}$  drill, then a  $5\text{mm}$ , a  $8\text{mm}$  and finally  $8.5\text{mm}$ . This was done to reduce the amount of axial force applied to the plies during the final boring procedure. After drilling two holes on the sample, as shown in Figure 29, a sample was cut in the middle of the drilled holes using a tile cutter wheel. The exposed cross sections were to be wet sanded, dried and then inspected with a  $40x$  optical microscope. The microscope was equipped with a CCD



Figure 29 –  $8.5\text{mm}$  holes drilled in  
8-ply CFRP-foam samples

sensor that allowed capturing of digital images. The samples were first polished on a 1200-grit paper then wet-polished on a 3000-grit polishing wheel, and the resulting difference is clearly visible in Figures 30 and 31, which was taken at the corner between the flat top and the sides of the sample. In Figure 31, it is possible to appreciate the CFRP strands exposed by appropriately angled lighting. The entire interface surface between the foam and CFRP was inspected seeking for voids or delamination between the

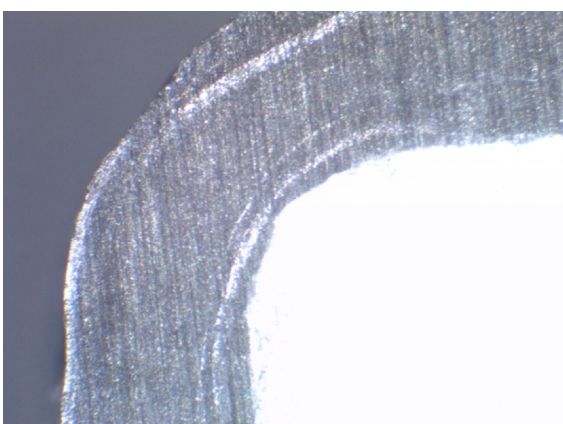


Figure 30 – 8-ply CFRP-foam sample cross-section  
cut polished with 1200-grit sanding paper

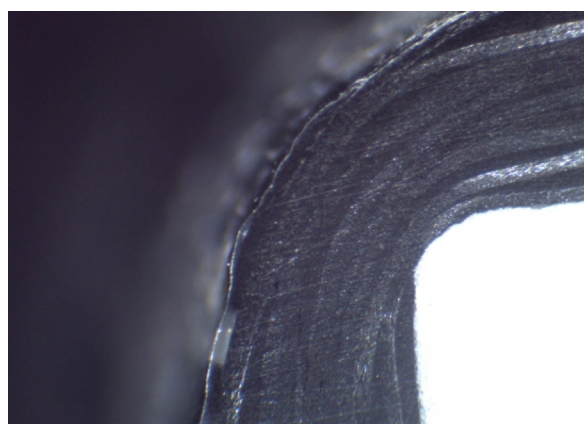


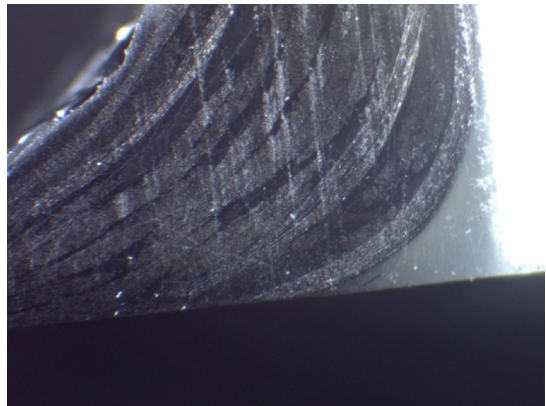
Figure 31 – 8-ply CFRP-foam sample cross-section cut  
polished with 3000-grit polishing wheel

two materials but none were found.

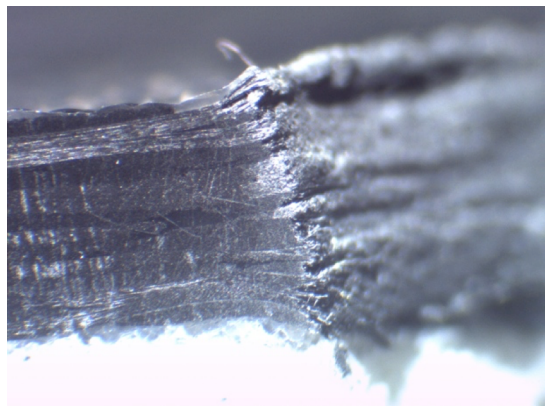
While inspecting the sample, it was noted that epoxy pockets were formed when the corner radius was smaller than 1mm, as it can be appreciated in Figure 32. Using the digital image-based ruler available in the image-capturing software the thickness of the plies was measured at  $1.774\text{mm}$ , equal to  $0.22\text{mm}$  per ply.

Figure 33 shows the interrupted cross-section where it meets with the bore of the hole.

Delamination of the carbon strands between the plies is visible, as well as pulled-up fibres close to the top from the drilling and pushed-through fibres in the bottom ply due to axial force applied when drilling. By using the digital ruler this affected zone was measured at around  $0.3\text{mm}$ . Figure 34 shows the CFRP bore surface; Through-thickness damage is even more apparent but still contained within fibre strands and no large delamination between plies is visible. Given the intent to bond the studs in the bore it is expected that the adhesive will partially fill the voids formed by the drilling procedure and regain some lost strength in the composite.



*Figure 32 – 8-ply CFRP-foam sample cross-section – CFRP bridged between foam and PTFE table during curing and epoxy pocket formation.*



*Figure 33 – 8-ply CFRP-foam sample cross-section – CFRP bore edge damage due to drilling procedure.*

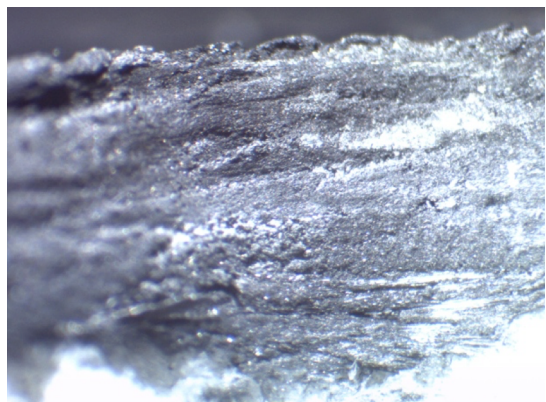


*Figure 34 – 8-ply CFRP-foam sample cross-section – CFRP bore damage due to drilling procedure.*

## 5.4 Shear testing

### 5.4.1 Yield Strength

The cured samples from the main batch were extracted from the bag and released from the film.

Figure 35 shows a detailed view of a 12-ply sample beside an 18-ply sample. An accumulation of epoxy is visible on the centre portion of the 18-ply sample, which could be attributed to the laminate being compressed harder at the edges forcing more epoxy to lower pressure areas like the top face.

As per the test setup, steel plates needed to be bonded to each side of the samples, so they were prepared for bonding, as shown in Figure 36. The bonding agent chosen was Permabond ET5429, an engineering adhesive with a shear strength of 18-22MPa with mild steel. Due to time constraints and concerns of failure of the adhesive (predicted shear stress with a 9kN load of around 12MPa), the samples were cured with the steel plates and studs in an oven at 60° for 2 hours to reach full strength, obtaining the result visible in Figure 37. The test assembly was completed by fitting of the adapters to use spherical rods and mounted on a Shimadzu tensile machine. The first sample of each ply/foam combination was to be tested to failure,



Figure 35 – Cured CFRP/foam samples: 12-ply (left) and 18-ply (right)



Figure 36 – Steel plates roughened and ready for bonding



Figure 37 – Stud and steel plates successfully bonded to the test sample with aluminium fitting

which was targeted at a factor of safety of 3. Using the force value calculated in Equation 20 the resultant force to be achieved was approximately  $9kN$ . The test setup mounted on the tensile machine, displayed in Figure 38, was set to perform a single cycle test at  $2mm/s$  with limit at  $10kN$ .

Unfortunately during the first run of the test, on sample HERO110/01 during preloading a small gap opened between the sample and the aluminium stud retainer. The stud was no longer loaded in pure shear and failed by bending stress at approximately  $5500N$ . In order to avoid this issue the subsequent samples were loaded to a load of approximately  $50N$  using manual position control and then the two mating faces pressed together. The results from these tests are overlaid on the chart in Figure 39.



*Figure 38 – Full wheel stud test assembly mounted on Shimadzu tensile machine*

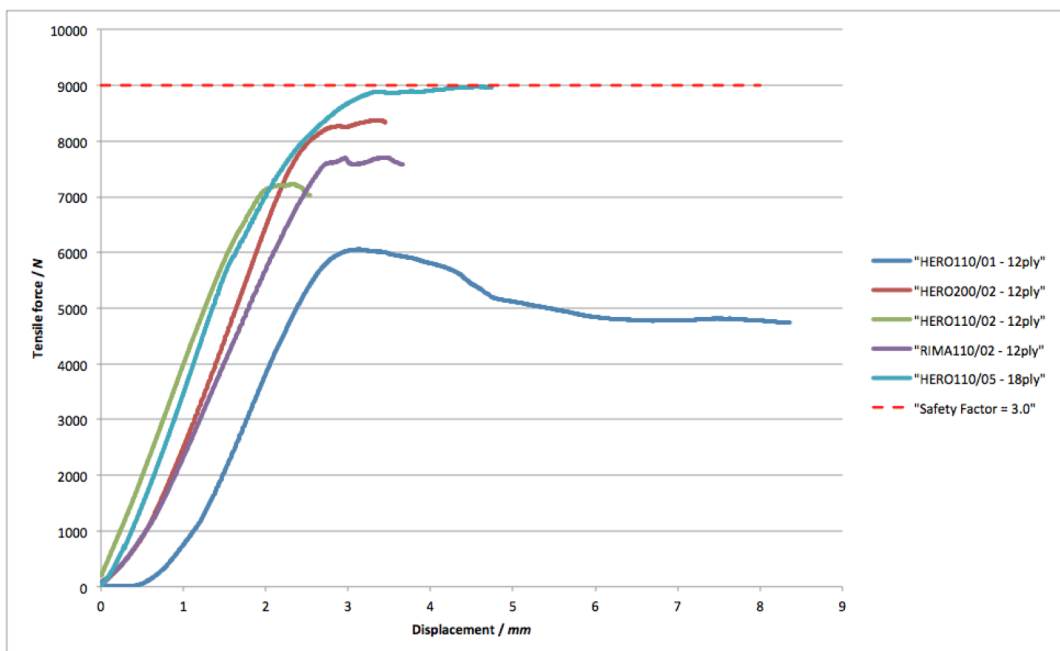


*Figure 39 – CFRP/foam test samples load to failure*

The HERO200/02 and RIMA110/02 samples showed yield failure at around  $7.5kN$ . The failure mode of the samples was deemed to be due to rotation of the pin inside. The HERO110/05, an 18-ply CFRP sample, was tested next and yielded at around  $8kN$ . Inspection of the failure showed that the assembly failed due to shear of the stud, as shown in Figure 40. Later calculations showed that shear stress on a 8.5mm stud equaled to a shear stress of  $141MPa$ . The alloy of the aluminium stud was unknown but datasheets (ASM, 2016) show that

alloys vary from  $100-350MPa$ . Due to a lack of time available to manufacture a pin out of higher-grade aluminium or steel and a demonstration that the sample exceeded the safety factor of the studs used on the Formula SAE car (which can now be evaluated at a factor of safety of 2.8 based on this study's load case) it was decided that the 18-ply HERO110 sample has passed the test, as the studs used for this test that were machined from the same aluminium rod as the ones used on the car had failed before the CFRP-foam. Testing the HERO200 sample was unnecessary and it was decided to use the remaining pin to evaluate the sample HERO110/02, to obtain a direct comparison between it and the equal foam density RIMA110/02. A suspicion that the non-linearity observed in the first 4 tests was due to play in the fasteners and rotation of the visibly-bent spherical rod bolts was confirmed by loading the HERO110/02 sample to  $100N$  manually then releasing the play by movement of the assembly and bolts. The load-displacement graph in Figure 39 is far more linear but failed at the lowest load of  $7kN$ , again due to rotation of the pin pivoting on the carbon skin.



Figure 40 – HERO110/05 sample post-test failure inspection

Based on these results it was accepted that whilst the 12-ply samples have almost achieved the same strength as the aluminium stud's shear strength, there was an insufficient number of samples tested to evaluate the divergence in strength between samples and the possible weakening of the CFRP bore due to drilling of holes in close proximity to one another like that of the wheel interface (Figure 19).

For this reason, an 18-ply layup is suggested for the wheel-axle interface, using either HERO 110 or RIMA 110 rigid foam core in the region of the bore of the wheel.

#### **5.4.2 Cyclic testing**

A cyclic, fatigue-like test was run on a sample identical to that which caused the shearing of the pin, on sample HERO110/04. The test should provide insight into whether repetitive application of tensile force could cause accumulated damage and begin cracks between the bonded stud and the CFRP-foam test sample. Unfortunately, due to the design of the test assembly it was not possible to apply compressive forces in alternation to tensile ones, but the test ran from almost fully relieved (below  $200N$ ) to a target load. During operation on the car the CFRP wheel will undergo rapid changes in torque so the machine was set for this experiment at  $20mm/s$ , the highest velocity that could be achieved before the tensile machine PID controller overshot target forces too greatly. Two short tests were run due to limited time available on the tensile machine: one with 100 cycles oscillating between  $50N$  and  $4500N$  and the other 50 cycles between  $200N$  and  $6000N$ . Force-Displacement plots of these two tests are available in Figures 41 and 42. The plots, albeit hard to read due to overlaying lines, show no sign of increase in displacement apart from the first cycle on the second test, where the play is removed. The sample was then tested for yield strength, to identify if any weakening of the part had occurred during cyclic testing. The result, visible in Figure 43, purposely yielded the test sample to assess the ability of the CFRP wheel assembly to withstand loads that exceed

the cases calculated in Section 3. Thanks to the shearing of the studs instead of CFRP damage the failure was progressive and stayed above yield strength.

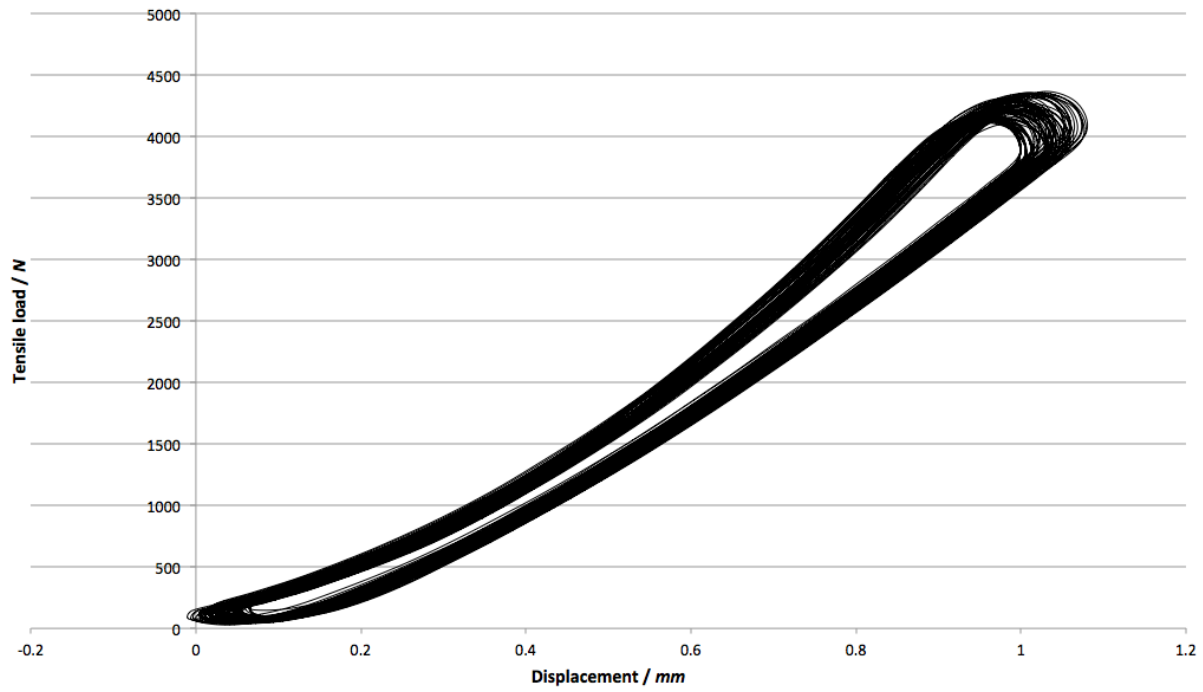


Figure 41 – HERO110/04 Test sample cyclic loading test 1 load-displacement curve

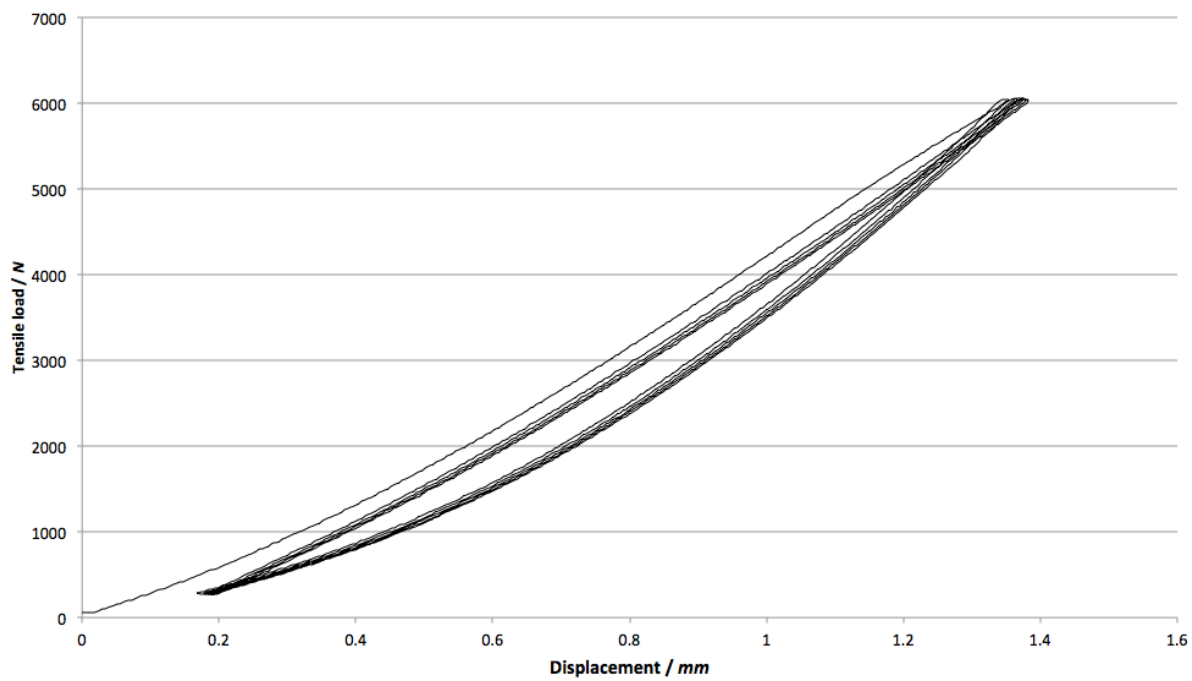


Figure 42 – HERO110/04 Test sample cyclic loading test 2 load-displacement curve

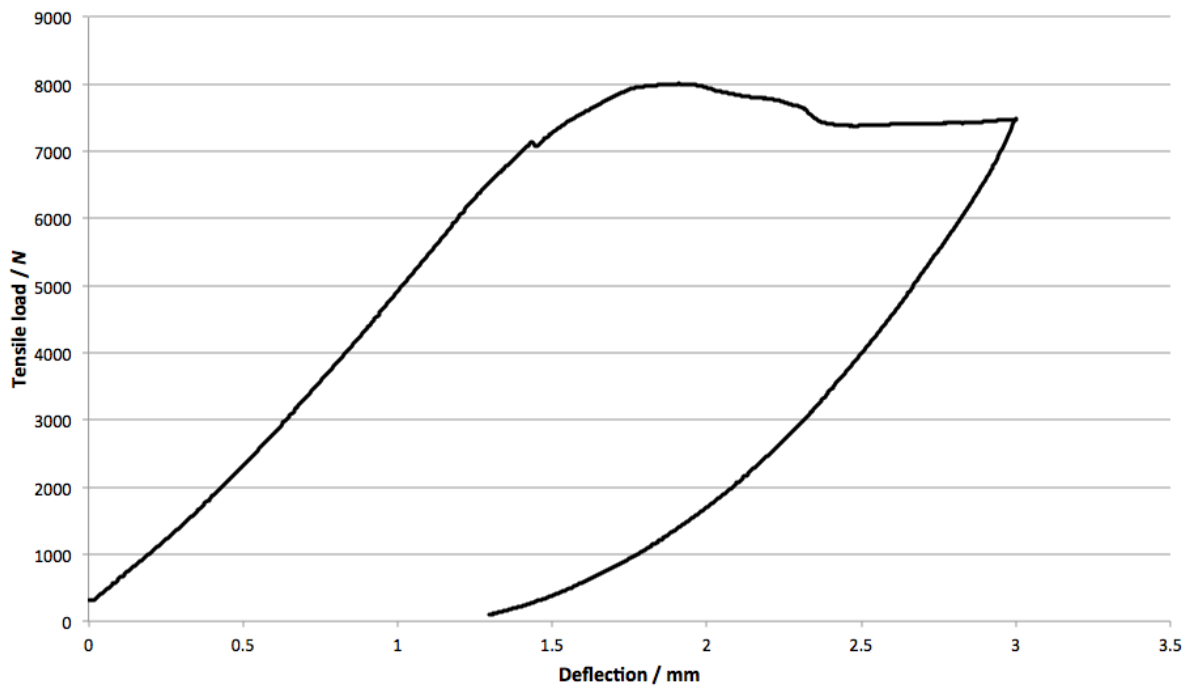


Figure 43 – HERO110/04 Test sample post-cyclic loading yield load-displacement curve

## 6. Computational Simulation

When performing Finite Element Modeling, hereinafter referred to FEA, there are several software packages available to the engineer to perform analysis on composite structures. The software made available for this project via the resources of the university and Cardiff Racing included Abaqus, Patran and Altair Hyperworks. While all featured their own advantages, Abaqus was chosen over the others due to its popularity in academia, meaning that help could be easily found between members of staff of the university. Several examples of good correlation between Abaqus models and experimentation were found, including failure path prediction (Bogert et al., 2006) and failure modeling (Svard, 2012). It also featured the ability to write and run scripts and easily control the ply stack and orientation of the CFRP.

### 6.1 Case setup, Boundary Conditions and Load definitions

As previously discussed, the proposed wheel will be manufactured from CFRP and Rohacell rigid foam. The CFRP material available for this project was limited to  $200\text{g m}^{-3}$  2x2 twill woven prepreg cloth. Due to woven CFRP's strong anisotropic behavior, as demonstrated by Vallons et al. (Figures 44 and 45) it was not possible to model a woven material like that which will be used to manufacture the wheel. For this reason it was necessary to create a unidirectional CFRP material (Appendix D) based on the same fibre and matrix compositions as that of the woven material, then manually ply the carbon in orthogonal directions when specifying the laminate layup. In order to avoid orthotropic stiffness it was decided that a ply of 0/90 weave, measuring 0.22mm thick as measured earlier,

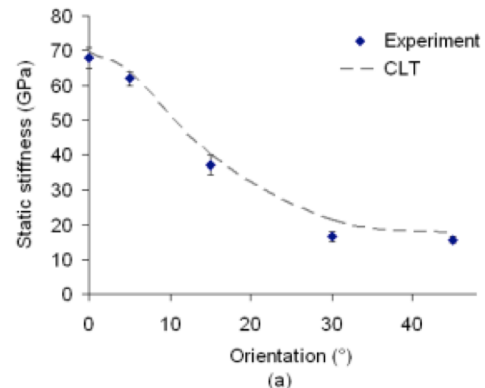


Figure 44 – Tensile test results for the different laminate orientation angles; stiffness compared to theoretical values (K. Vallons et al.)

would be represented by a sandwich composed of 0.055mm unidirectional fibre at 0 degrees, 0.11mm at 90 and a 0.055mm ply at 0 degrees. This is essentially a 0/90/90/0 layup and was chosen over a 0/90/0/90 due to the presence of bend-twist effects on the latter layup. Theoretically the weave could have been divided into infinitely small plies but excessive complexity of the ply stacks limited these plies to three.

As calculated in Section 3, the wheel would need to be loaded from the point of contact of the tyre with the ground and constrained at the axle interface. Displayed in Figure 46 is

the CAD representation of the CFRP wheel loaded in the Abaqus display port showing the reference point “constraint point” applied to the bore and axle face of the wheel. As explained in earlier section, the wheel studs will not be simulated and instead the entire face will be constrained to rotations in the  $y$ -axis. The axle bore was restrained

from moving in either the  $x$  or  $z$ -direction, and the  $y$  translations were constrained by the axle face and the face on which the wheel nut sits. A reference point was applied at 203.6mm

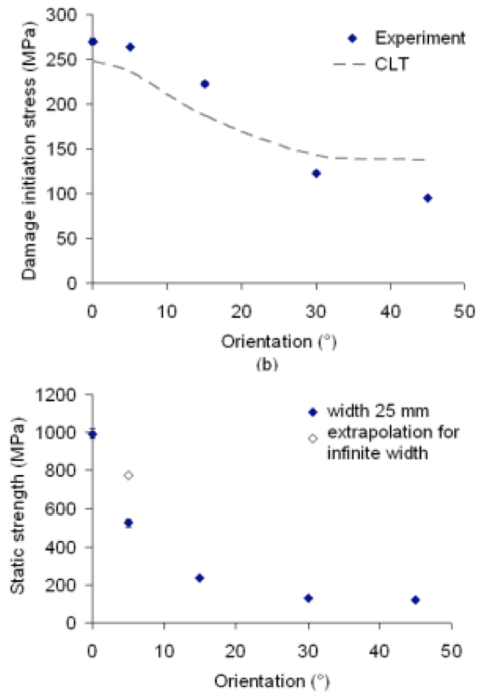


Figure 45 – Tensile test results for the different laminate orientation angles; stress to damage initiation and strength (K. Vallons et al.)

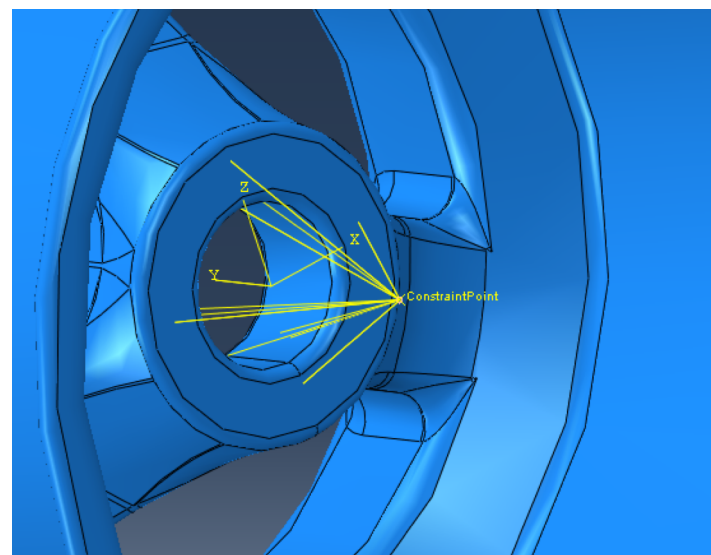


Figure 46 – CFRP wheel in Abaqus; Constraint between the wheel bore and axle face and a reference point “Constraint Point”

below the centre of the wheel, equal to the radial measurement of the Avon tyre used by Cardiff Racing. This point was constrained to the lip of the wheel, as this was the surface through which the tyre applies its forces (Figure 47).

## 6.2 Evaluation of Keizer wheels

In order to correctly evaluate the CFRP wheels as a replacement to the Keizer wheels, an identically constrained and loaded case was set up for the three-piece aluminium wheels. These were assigned a solid section of 6061-T6 aluminium with a Young's modulus of  $69GPa$  and a Poisson's ratio of 0.33. The faces of the three pieces that compose the wheel were mated and the load from the worst-case load from Table 2 was applied to the wheel. A field output of Von Mises stress can be viewed in Figure 48, where a color field range from 0 to  $375MPa$  was applied. Maximum stress is reached inboard of the wheel on the spokes (Figure 49), where the stress concentration closely resembled the result of a dye-penetrant crack test on a set of two-year old wheel centres found cracks in the arms (Figure 50).

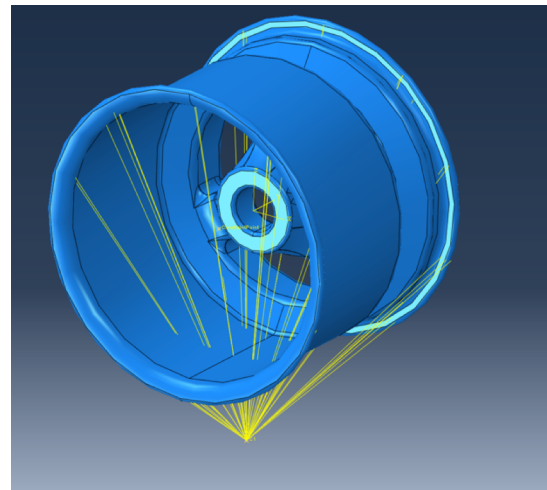


Figure 47 – CFRP wheel in Abaqus; Constraint between tyre contact patch reference point and wheel lips

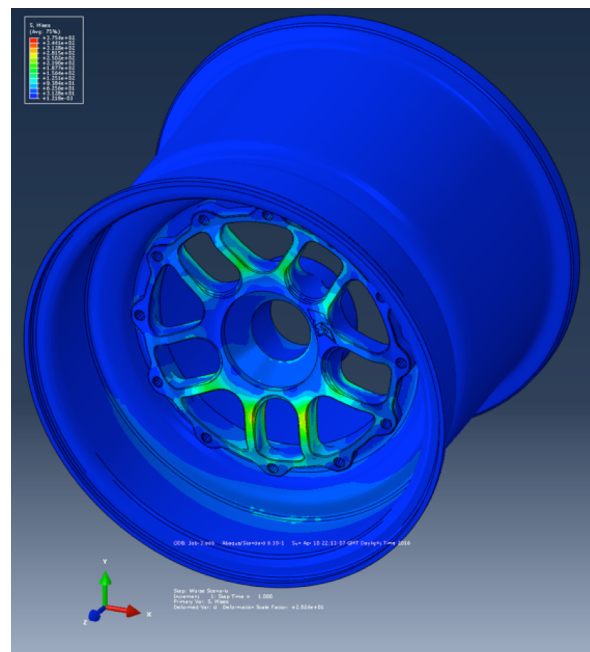
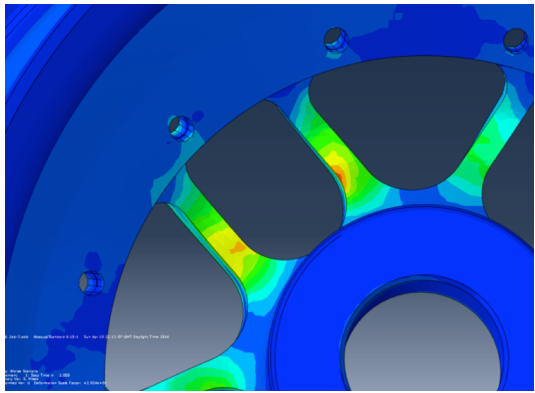


Figure 48 – Keizer wheel in Abaqus; Von Mises field output on worst-case load scenario. Color field from 0 to  $375MPa$



*Figure 49 – Keizer wheel in Abaqus; Von Mises field output stress concentration on worse load case scenario. Color field from 0 to 375MPa*



*Figure 50 – Keizer wheel centre inboard side; result from dye-penetrant crack testing showing hairline cracks developing on spoke roots*

The yield stress of 6061-T6 is around 276MPa (ASM, 2016) so according to the simulation the Keizer wheel centre would fail under the loading. This did not occur on the Formula SAE vehicle because the load case calculated simulates a vehicle that is 20kg heavier, runs an aggressive high lift aerodynamics package and utilizes slightly higher grip tyres. Nonetheless, the stress concentration still persists and the model and load case can be partially validated thanks to correlation with the crack locations. An additional metric was measured from the case, which is dilution of camber: under the load it was calculated that the wheel lip twisted 0.45° relative to the axle.

### **6.3 Simulation and development of CFRP wheel**

The wheel proposed in this report is composed of a solid foam core and laminate CFRP skins. In order to model this correctly, the wheel was imported from CAD as a solid and assigned the material property of HERO 110 foam to its volume. Skins, an Abaqus native method for defining shell elements on solid bodies, were used on the CFRP wheel surfaces. In line with the design intent to optimize the wheel via specification of diversified layups for the various surfaces, a number of skins were defined and assigned to regions of the wheel such that each

could be assigned a distinct layup. During the first few sessions of development 14 different skins were defined and each assigned a specific laminate stack in order to be able to control and minimize the plies in lower stress regions. Each of these skins was assigned an orientation control in order to accurately control the reference directions with which the plies were defined. Concerns of significant changes in stress levels and paths as the wheel revolved meant that it was deemed necessary to apply the load at several points. This was done by use of rotated reference frames about the  $y$ -axis (the wheel's rotation axis), which allowed for direct comparison of vertical and longitudinal deflections in the wheel. A study in the effect of increased mesh density and its accuracy effects on solve time was performed. It revealed that a cell count of around 400'000 and a face count of 100'000 offered a sufficiently quick job solve time of around 60s per step (Static, General step) and a very good resolution. An attempt to automate the process of developing the wheel by means of writing a script based on a genetic algorithm to optimize the wheel was unsuccessful due to difficulties with indexing and reading the field output maxima locations, the very large time complexity of the algorithm (estimated to require at least one month on a modern workstation) and likelihood that the output would produce a layup almost impossible to manufacture. Each design iteration was thus performed and evaluated manually. This proved to be very time consuming with the original number of skins and over the course of around 50 iterations of modification of plies based on stress levels, CFRP skins with similar sections were merged into a single skin. The resulting reduced number of skins defined can be seen in Figures 51, 52, 53, 54 and 55.

As proven by experimentation, it was necessary to utilize the ply layup [0/30/60]<sub>3s</sub> on the axle face, where the CFRP would be drilled to fit and captivate the wheel studs. For the first case using 5 skins, on the inboard surface it was considered that the stress would have been low, so a 4-ply balanced layup of [0/45]<sub>2</sub> was utilized. For the remaining portions of the wheel the layup was a 6-ply [0/30/60]<sub>s</sub>. It is important to note that the layup stacks described specify the angle of the warp fibers, where the weft fibers are maintained at an orthogonal angle to the warp ones (see Figure 56 for the Abaqus laminate definition for a [0/30/60]<sub>s</sub>).

A case utilizing this layup was tested at a rotation angle of 0°, 30°, 60° and 90°. The results were mostly analyzed by field output of Tsai-Hill criterion utilizing a color range between 0.25 and 0.01. As described by Kolios et al. (2012) the safety factor is equal to  $1/\sqrt{\text{Tsai Hill}}$  equalling a factor of safety of 2 and 10 respectively,

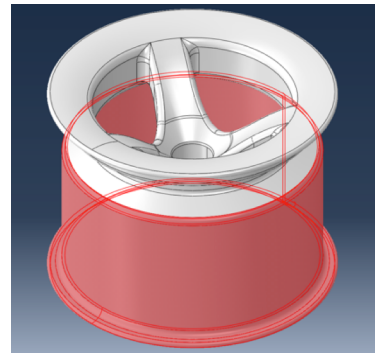


Figure 51 – CFRP wheel “inboard” skin surfaces

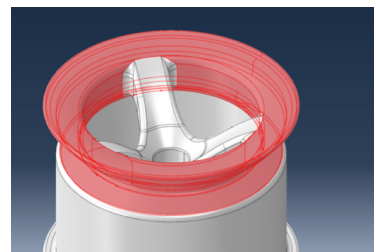


Figure 52 – CFRP wheel “outboard” skin surfaces

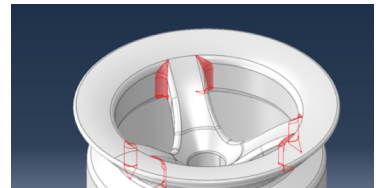


Figure 53 – CFRP wheel “spoke joints” skin surfaces

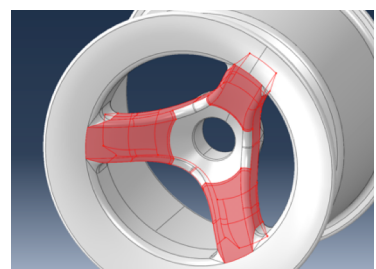


Figure 54 – CFRP wheel “spokes” skin surfaces

| Edit Section  |           |                   |                    |          |
|---|-----------|-------------------|--------------------|----------|
| Name: AxlePly<br>Type: Shell / Continuum Shell, Composite<br>Section integration: <input checked="" type="radio"/> During analysis <input type="radio"/> Before analysis<br>Layup name: 0/30/60 |           |                   |                    |          |
| <input checked="" type="checkbox"/> Symmetric layers  |           |                   |                    |          |
| Material  | Thickness | Orientation Angle | Integration Points | Ply Name |
| CFRP  | 0.055     | 0                 | 5                  | L1a      |
| CFRP  | 0.11      | 90                | 5                  | L1b      |
| CFRP  | 0.055     | 0                 | 5                  | L1c      |
| CFRP  | 0.055     | 30                | 5                  | L2a      |
| CFRP  | 0.11      | 120               | 5                  | L2b      |
| CFRP  | 0.055     | 30                | 5                  | L2c      |
| CFRP  | 0.055     | 60                | 5                  | L3a      |
| CFRP  | 0.11      | 150               | 5                  | L3b      |
| CFRP  | 0.055     | 60                | 5                  | L3c      |

Figure 56 – Abaqus input for a [0/30/60]<sub>s</sub> layup; note the “symmetric layers” option active

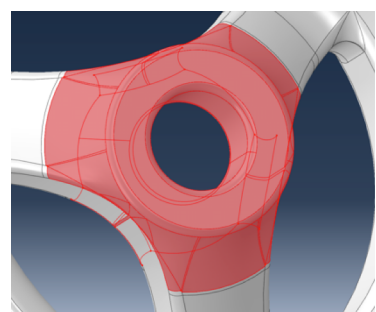
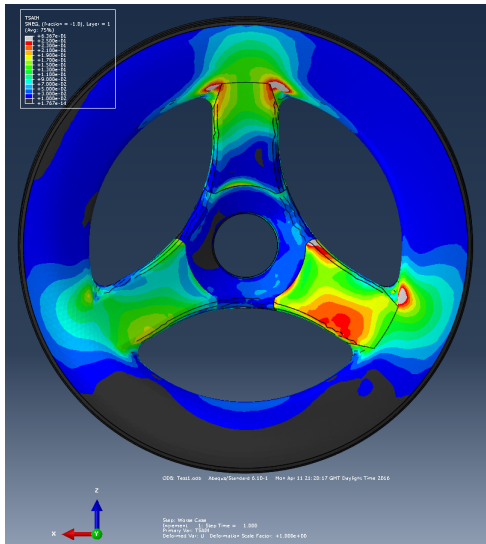


Figure 55 – CFRP wheel “wheel centre” skin surfaces

meaning that areas that exceed the range (light gray) are regions that are below target factor of safety and should be evaluated for change in ply orientation or increase in count.

Alternatively, regions that are black exceed a factor of safety of 10, meaning they can be made lighter by removal of plies. Figures 57, 58, 59, 60 show the field output of Tsai-Hill factor on the outer face when the force is applied at different radial points to simulate different wheel positions.



*Figure 57 – CFRP Wheel Case 1 with load point rotated 0 degrees; Tsai-Hill field output using color range [0.01, 0.25]*

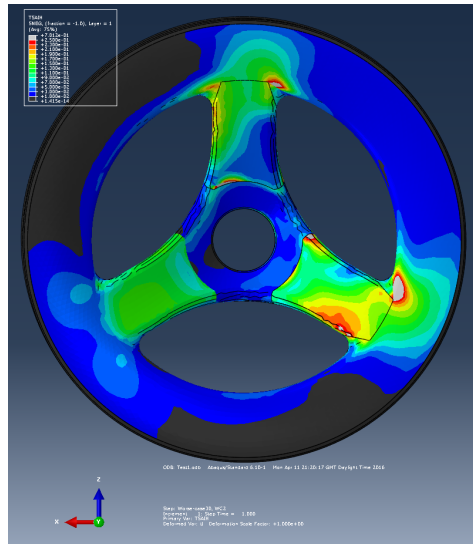


*Figure 58 – CFRP Wheel Case 1 with load point rotated 30 degrees counterclockwise; Tsai-Hill field output using color range [0.01, 0.25]*

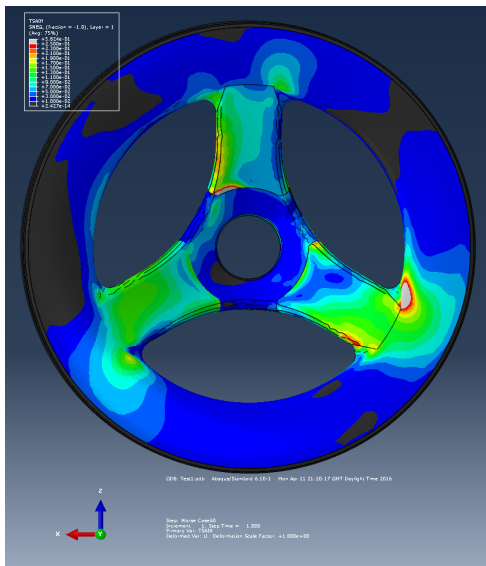


*Figure 59 – CFRP Wheel Case 1 with load point rotated 60 degrees counterclockwise; Tsai-Hill field output using color range [0.01, 0.25]*

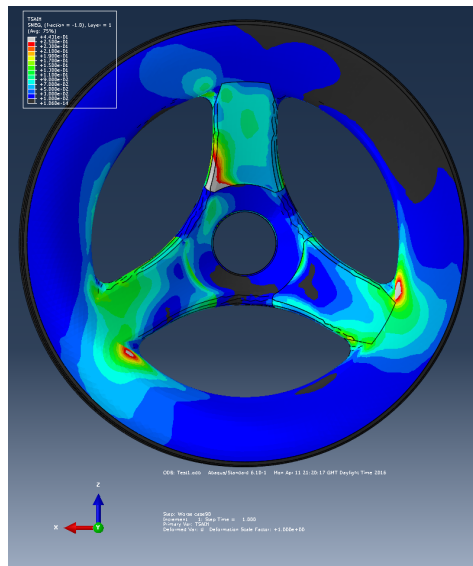


*Figure 60 – CFRP Wheel Case 1 with load point rotated 90 degrees counterclockwise; Tsai-Hill field output using color range [0.01, 0.25]*

The maximum value of Tsai-Hill obtained in Case 1 largely exceeds 0.25, meaning reinforcement of the affected areas is clearly necessary on the spokes. Figures 57, 61 show that this value is exceeded on several surfaces of the spokes and partially on the outboard wheel face. The spokes also contributed to a large rotation of the wheel in the  $x$ -axis, equivalent to a reduction in negative camber of  $0.55^\circ$ . The spokes were reinforced for Case 2 using a  $[0/30/60]_{2s}$  (Figure 62). A reduction in deformation was observed for a weight increase of  $36g$ , so a further increase to  $[0/30/60]_{3s}$  (Figure 63) was done to make the wheel even stiffer. The outboard wheel hoop surface was still failing to meet target safety factor so an increase to  $[0/45]_{2s}$  and successively  $[0/30/60]_{2s}$  was necessary to pass. Ply count was not modified on either the wheel centre or the inboard wheel drum, but a re-orientation of the plies in the latter was performed to reduce deflection in the  $y$ -axis. Orientation of these to  $[0]_4$  aligned the fibres to the wheel axis proved to be the stiffest ply stack and reduction in ply

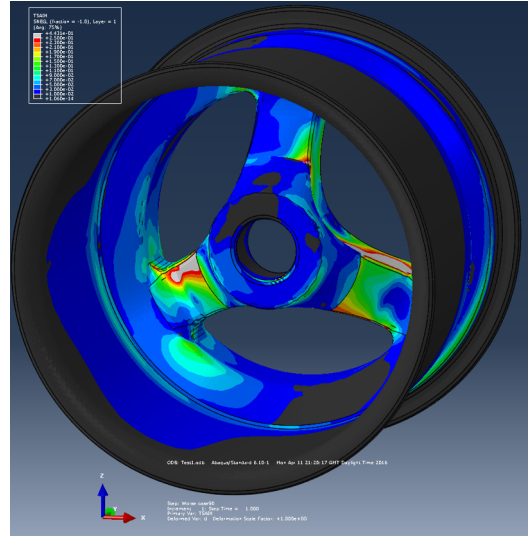


*Figure 61 - CFRP Wheel Case 1 with load point rotated 0 degrees; Tsai-Hill field output using color range [0.01, 0.25]; Inner view*

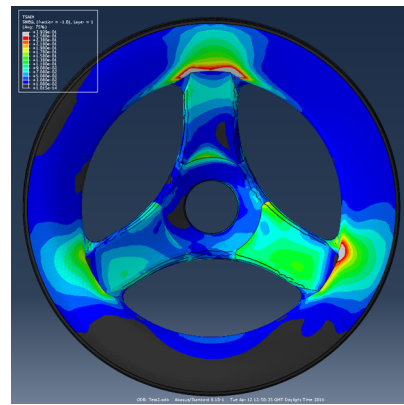


*Figure 62 - CFRP Wheel Case 2 with load point rotated 0 degrees; Tsai-Hill field output using color range [0.01, 0.25];*

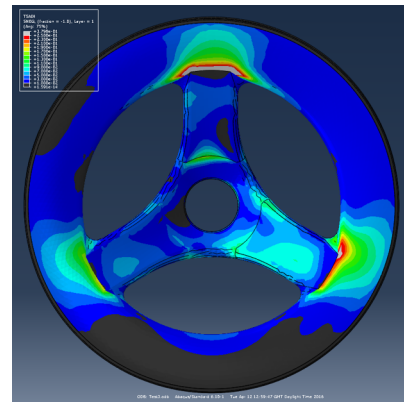


*Figure 63 - CFRP Wheel Case 3 with load point rotated 0 degrees; Tsai-Hill field output using color range [0.01, 0.25];*

count down to [0]₂ gave significant weight savings in Case 9.

The stress in the foam core, monitored as

a Von Mises metric, was observed

throughout the various iterations and it

was progressively less stressed as the ply

count was increased on the wheel. This is

likely due to an increase of the bending

moment carried by the skins directly. The

core's factor of safety exceeded 3.0 in any

iteration and is equal to 5.6 on the final

layup case (Figure 64). Based on this value

it was considered worthy to evaluate the use of lower density foam, namely HERO 71 foam.

This is less dense ( $75\text{kg m}^{-3}$ ) and less stiff ( $123\text{MPa}$ ) but weighs 49g less and costs less. The

result was minimal stress change in the skins (Safety factor reduction of 2%) and reduction in

wheel stiffness by 3%. Unfortunately the stress increased to exceed the maximum compressive

stress of HERO 71 and would fail. The change in stiffness observed in the lower core density

case prompted interest in evaluating the heavier HERO 150 and HERO 200 cores. These

increased the stiffness of the wheel by 2% and 4% and were much stronger than necessary,

with a safety factor of 8.2 and 14.1 respectively.

A summary of all the cases run on the 5-skin CFRP wheel is available in Table 3, where a description of the change and relevant metrics is available for each. Weight was calculated by using the surface area of each skin and multiplied by the number of plies and the weight of the prepreg cloth (200g) and the volume of the wheel by the density of the foam used. Table 4 offers a breakdown of the contribution of each portion of the wheel for case 12.

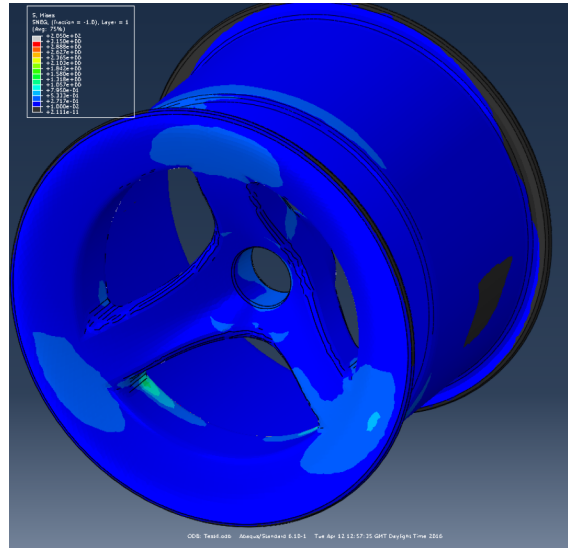


Figure 64 - CFRP Wheel Case 9 with load point rotated 0 degrees; Foam core Von Mises field output using color range [0, 3]. Maximum stress 1.4MPa

*Table 3 – Summary of CFRP wheel cases and relevant performance metrics*

| Case number and description  | Lowest Safety Factor | Rotation in $x$ -axis / ° | Weight / g |
|--|----------------------|---------------------------|------------|
| <b>Case 1</b> – “Inboard” at [0/45] <sub>2s</sub> ; “Outboard”, “Spokes” and “Spoke Joints” at [0/30/60] <sub>s</sub> ; “Wheel Centre” [0/30/60] <sub>3s</sub> ; HERO 110 core | 1.186                | 0.551                     | 605.8      |
| <b>Case 2</b> – As Case 1 but “Spokes” and “Spoke Joints” with [0/30/60] <sub>2s</sub>   | 1.59                 | 0.474                     | 641.8      |
| <b>Case 3</b> – As Case 1 but “Spokes” and “Spoke Joints” with [0/30/60] <sub>3s</sub>   | 1.62                 | 0.416                     | 677.7      |
| <b>Case 4</b> – As Case 3 but “Outboard” with [0/45] <sub>4s</sub>   | 1.68                 | 0.351                     | 732.1      |
| <b>Case 5</b> – As Case 3 but “Outboard” with [0/30/60] <sub>2s</sub>  | 2.18                 | 0.319                     | 840.9      |
| <b>Case 6</b> – As Case 5 but “Inboard” with [0/45] <sub>3s</sub>  | 2.18                 | 0.277                     | 934.4      |
| <b>Case 7</b> – As Case 5 but “Inboard” with [0] <sub>4s</sub>   | 2.19                 | 0.278                     | 840.9      |
| <b>Case 8</b> – As Case 5 but “Inboard” with [0] <sub>3s</sub>   | 2.18                 | 0.290                     | 794.2      |
| <b>Case 9</b> – As Case 5 but “Inboard” with [0] <sub>2s</sub>   | 2.18                 | 0.296                     | 747.4      |
| <b>Case 10</b> – As Case 9 but HERO 71 core  | 0.91                 | 0.302                     | 697.9      |
| <b>Case 11</b> – As Case 9 but HERO 150 core   | 2.23                 | 0.290                     | 804.0      |
| <b>Case 12</b> – As Case 9 but HERO 200 core   | 2.28                 | 0.284                     | 874.8      |

*Table 4 – Summary of CFRP wheel cases and relevant performance metrics*

| Surface       | Area / mm <sup>2</sup>   | Ply count                    | Weight / g |
|---------------|--------------------------|------------------------------|------------|
| Inboard       | 233685                   | 2                            | 93.5       |
| Outboard      | 135982                   | 12                           | 326.4      |
| Spokes        | 26133                    | 18                           | 94.1       |
| Spoke joints  | 3840                     | 18                           | 13.8       |
| Wheel centre  | 17794                    | 18                           | 64.1       |
| <hr/>         |                          |                              |            |
| Body          | Volume / mm <sup>3</sup> | Density / kg m <sup>-3</sup> | Weight / g |
| HERO 110 Core | 1415749                  | 110                          | 155.6      |
| <hr/>         |                          |                              |            |
| <b>Total</b>  |                          |                              | 747.4      |

## 7. Project Discussion

The lightest CFRP wheel that exceeded factor of safety of 2 on all load cases and showed high levels of stiffness is Case 9 and theoretically weighed 0.7474kg. This value is likely going to be slightly different in a manufactured wheel. The core will not be as volumetrically large as the original CAD part as a small quantity of foam will be removed from its surface equivalent to the thickness of the CFRP skins. One can estimate the weight loss by using the area covered by each skin, multiply it by the number of plies and the thickness of a ply. This calculation is inaccurate, as it doesn't take into account that convex surfaces will shrink by a certain value for every ply removed but it returns a weight reduction of 71.6g. The same task, performed on CAD, yields a weight reduction of around 40g. The wheel would also be heavier due to the need to strengthen the wheel lip for assembly and the amount of CFRP overlap to join surfaces made from different cuts of CFRP and to join areas of the wheel that have different ply orientation or count. This wheel compares well with the literature investigated, though it is important to remember that the load cases utilized, strength metric used and safety factor are different for each author. Ressa's (2013) lightest wheel weighed 0.783kg, used a load case with 12% more  $F_z$ , 40% less  $F_x$  and 70% less  $F_y$  and deflected 0.21°. Thanks to a foam core, the wheel proposed in this dissertation will weigh almost the same but will only deflect 50% more with a lateral load that is 230% higher. Uyttersprot (2015) uses a similar load case, except with higher vertical load and achieves a weight for a one-piece wheel of 1.500kg using a single specification of plies for the entire wheel. This is sub-optimal as most regions of the wheel are well below stress limits. This weight would be similar to that of the CFRP wheel proposed in this dissertation if the maximum number of plies (18) were to be applied to all the skins (1.658kg). The design compares well to Competitors' wheels like AMZ Racing and TU Graz, being around 100g lighter than each and is lighter than the hybrid aluminium-CFRP wheels like those of Team Bath Racing.

The wheel surface was largely defined by the current suspension and upright geometries. If the Team were to redesign the assembly and allow freedom the geometry would have been different. The front brake caliper, at 3mm from the inner wall of the wheel, and other assemblies would have been moved to allow for a thicker foam core in the inboard wheel drum and potential improvements in stiffness. The large distance between the wheel nut seat and the outer lip of the wheel would have been reduced to allow stronger wide-spoke geometries or full-disk wheel that were not possible due to excessive Gaussian curvature.

The load cases used were deemed accurate for future-proofing the CFRP wheel in case the car gained weight, increased its CG height or improved its cornering performance, but were far higher than loads currently experienced by the Keizer wheels. By use of the same calculation for the load case but using values from the 2015 car ( $250\text{kg}$ ,  $\mu = 1.25$ ,  $ClA = 0.8$ ), the vertical load is 53% lower, the lateral and longitudinal 61% lower than the proposed load case. This meant that a lighter wheel could have been manufactured using lower load values but it would have been necessary to limit the usage of the wheel to a car with specific maximum weight and aerodynamic load.

The moulds designed could be costly to manufacture: purchasing of the billet aluminium necessary to make all the parts had a quoted price of around 300 GBP and the manufacturing may cost even more, although it is hoped that a Team sponsor could perform the job for a lower fee. The estimated cost of a single wheel would be around 450 GBP: 100 GBP for the foam core, 50 GBP for the consumables (bagging film, breather cloth and release film) 300 GBP for the prepreg CFRP assuming a 50% tessellation efficiency ( $5.97\text{m}^2$  material consumption) in cutting the patterns and a 50 GBP/m<sup>2</sup> price for the material.

Observations made with the microscope (Figure 33 and 34) highlighted damage occurring around the drilled bore of the CFRP samples. As highlighted by Sakamoto et al (2007) the tool wear when drilling CFRP is very high. His studies show that a high speed steel tool

suffers far greater wear than a cemented carbide and only retains sufficient cutting ability up until a total depth of 27.8mm is cut in CFRP. Sakamoto et al. (2007) also investigate the rate of change in thrust force as different material twist drill wear and compares them in Figure 65. For this reason drilling should have

been performed only with new twist drills made preferentially from cemented carbide or DLC coated or that holes should be made with ball nose end mills at speeds of 300 m/min.

A very large deflection was observed during stud shear testing. This was

identified to deflection of the fixtures and steel plates, like the M5 bolts fitting in the spherical bearings visibly bending during testing. This prevented any ability to gain an understanding of the deflections occurring on the sample and could be tackled by using bigger spherical bearings, thicker steel plates and a larger bond surface on the sample or by use of local strain measurement methods like digital image correlation or properly located linear potentiometers. The shearing of the aluminium stud at  $8kN$  prevented measuring of the yield strength of the 18-ply sample; a steel pin could have been used to perform such test.

The remote reference point representing the tyre contact patch was accurate in the application of forces and moments to the wheel but forced the load to be applied in potentially incorrect manners. This may have caused a rotational deflection smaller than that which would be achieved with a real tyre fitted. The bore should also have been restrained by using a real axle to replicate the surface forces that a wheel would sustain during loading.

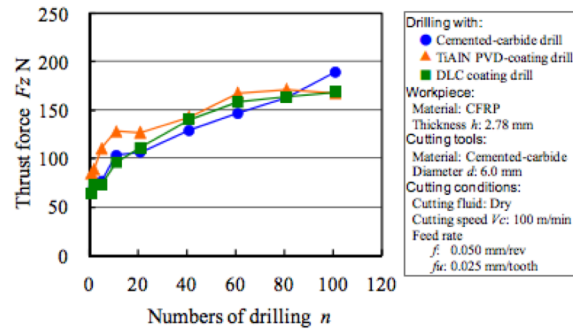


*Figure 65 – Effect of drilling numbers on thrust force of CFRP drilling processes with twist drills at  $V_c$  of  $100m\ min^{-1}$ , Extracted from Samakoto et al (2007)*

## 8. Project Conclusion

This project has successfully designed a wheel utilizing a rigid-foam core reinforced with CFRP skins. The proposed wheel was evaluated using numerical simulation and, where necessary, physical testing. Thanks to subdivision of the wheel into regions it was possible to optimize the layup and reduce ply count. This dissertation specifies a wheel design that theoretically weighs  $747.4g$  and has a safety factor of 2.18 on a limit load case in excess of that imposed by the current Cardiff Racing Formula SAE car. This was done to ensure that the CFRP wheel could be used in future years even if a significant increase in the forces applied to it by the car occurs, such as an increase in vehicle weight.

If the wheel proves to be strong enough once it is manufactured, it will provide a significant performance benefit to the team. The weight of the car would be reduced by  $6.6kg$  and the total inertia of the car including rotating masses by  $9.9kg$ . This translates to an improvement of 3.81% in acceleration, 1.27% traction-limited acceleration and 69% reduction in the gyroscopic inertia of the wheel. These will bring improvements in the Team's score in the Dynamic events, as well as gain points in the Design competition thanks to the use of parts designed and manufactured in-house. The team would also likely gain exposure with sponsors and peers thanks to owning the lightest wheel set in the entire Formula SAE competition (to the knowledge of the author, based on Teams' cars up to 2015). Their manufacturing will build upon Cardiff Racing's CFRP expertise and hopefully inspire the Team to perform research in the development of CFRP components in other areas of the car.

## 9. Further areas of study

The next major step toward utilization of the CFRP wheel on a Formula SAE car would be manufacturing: The moulds will need manufacturing, assembly, validation and refinement like the addition of alignment pins on the moulds. A cost reduction of the moulds may be achieved by design of near-net shape components for the large moulds, reducing the time and cost of machining and material waste. Based on the layup, the CAD for the foam core needs to be modified to allow for the thickness of the carbon skins. The cores will also need CNC machining so that it can be proven that the desired shape can be manufactured. The patterns required for layup will need to be generated either from CAD or experimentation on rapid prototyped surfaces. A tessellation study on the patterns is highly recommended as it would reduce waste of CFRP and reduce the cost and environmental impact. A study on a reduction in laminate damage may be performed by comparison of drilling techniques and drill material; any improvement should be validated by physical tensile tests similar to those run in this project. A further study into the practice of capturing studs in drilled CFRP could look at the effects of multiple holes drilled at a close distance to one another or attempt to reduce the ply count in the axle region by tackling the issue of pin rotation found in the 12-ply samples. This may be done by making a sandwich skin on the axle face such that the stud is retained by two skins: one at the surface and one at a small depth into the core. A testing setup that allows for two-way loading of the studs could also provide insights into possible fatigue behavior of the area and rectify these issues.

Once manufacturing of a wheel is done, it would be necessary to test the wheel under design conditions. A wheel test rig would need to be designed and manufactured, but the author suggests mounting a wheel with tyre and axle to a hydraulic press test machine at an angle from axis of rotation of the tyre equal to that of the vector drawn from the sum of  $F_y$  and  $F_z$ . This would be pressed onto a fixed highly abrasive surface inclined in the direction of travel

of the tyre at an angle equal to the vector drawn by the sum of  $F_x$  and  $F_z$ , thus simulating normal loading, lateral loading and longitudinal loading in the correct proportions.

An FEA model of the Avon tyre that in use by the team would prove beneficial to performing a more accurate load scenario on the CFRP wheel and could make findings into further weight reductions or identify stresses higher than measured in the model used in this project. Wheel lip load due to tyre pressure as well as adding the axle and upright to the assembly would further emulate the on-car conditions the wheel would be operating in.

A redesign in the surface of the wheel could also be performed to reduce the stress measured in the core that prevented the author from using the lower density HERO 71 foam.

Other studies should look at further optimization of the layup by use of unidirectional CFRP or non-crimp unidirectional CFRP as well as lighter-weight weaves. This could include writing a genetic algorithm for Abaqus such that the optimal layup would be found quicker or weight reductions found by division of the wheel surface in more regions. Alternatively the CFRP wheel could be modeled again in a laminate FEA package with an integrated optimization tool like Altair's Hyperworks.

## 10. Appendices

### A. 2x2 Twill CFRP data sheet



CONFIDENTIAL

#### CYTEC MATERIALS DATABASE

**MTM28 / T800 Carbon Fabric / CF1218**  
**Normalised to 55% Vf**

Source : ACG Technical Centre 2000 MRDB (J1046) + Routine QA

|   |   |              |          |  |  |
|---|---|--------------|----------|--|--|
| Material Details:   | MTM28/CF1218 – 200 gsm 6k T800 Carbon 2 x 2 Twill Prepreg               |              |          |  |  |
| Typical Processing:   | 120°C Autoclave Cure  |              |          |  |  |
| Characteristics:  | Highly toughened epoxy with 90°C maximum Tg. Can be cured down to 80°C. |              |          |  |  |
| Autoclave Cure Conditions for Data:   |   | 1 Hr @ 120°C |          |  |  |
| Postcure for Data:  |   | None         |          |  |  |
| Test Conditions for Data  |   |              |          |  |  |
| Property  | Test Method   | Units        | 20°C Dry |  |  |
| Tensile Modulus   | D 3039  | GPa          | 84.7     |  |  |
| Compressive Modulus   | D 3410  | GPa          | 73.4     |  |  |
| Trans. Tensile Modulus  | D 3039  | GPa          | 79.4     |  |  |
| Trans. Comp. Modulus  | D 3410  | GPa          |          |  |  |
| Tensile Strength  | D 3039  | MPa          | 1199     |  |  |
| Compressive Strength  | D 3410  | MPa          | 698      |  |  |
| Trans. Tensile Strength   | D 3039  | MPa          | 1140     |  |  |
| Trans. Comp. Strength   | D 3410  | MPa          |          |  |  |
| Tensile Strain to Failure   | D 3039  | %            | 1.39     |  |  |
| Comp. Strain to Failure   | D 3410  | %            |          |  |  |
| Trans. Tensile Strain   | D 3039  | %            | 1.44     |  |  |
| Trans. Comp. Strain   | D 3410  | %            |          |  |  |
| In-Plane Shear Modulus  | D 3518  | GPa          | 3.35     |  |  |
| In-Plane Shear Strength   | D 3518  | MPa          | 128      |  |  |
| Maj. Tensile Poisson's Ratio  | D 3039  | -            | 0.05     |  |  |
| Maj. Comp. Poisson's Ratio  | D 3410  | -            |          |  |  |
| Min. Tensile Poisson's Ratio  | D 3039  | -            | 0.05     |  |  |
| Min. Comp Poisson's Ratio   | D 3410  | -            |          |  |  |
| Flexural Modulus  | CRAG 200  | GPa          | 70       |  |  |
| Flexural Strength   | CRAG 200  | MPa          | 1321     |  |  |
| ILSS  | D 2344  | MPa          | 72       |  |  |
| All fabric data normalised to 55% fibre volume fraction (except for ILSS and In-Plane Shear). |   |              |          |  |  |

## B. ROHACELL rigid foam datasheets

| Physical properties  |             |                   |                   |                    |                    |                    |
|----------------------|-------------|-------------------|-------------------|--------------------|--------------------|--------------------|
| Property             | Test method | Unit              | ROHACELL® 71 HERO | ROHACELL® 110 HERO | ROHACELL® 150 HERO | ROHACELL® 200 HERO |
| Density              | ISO 845     | kg/m <sup>3</sup> | 75                | 110                | 150                | 205                |
| Tensile strength     | ISO 527-2   | MPa               | 4.1               | 6.3                | 8.8                | 12.3               |
| Tensile modulus      | ISO 527-2   | MPa               | 123               | 189                | 269                | 389                |
| Elongation at break  | ISO 527-2   | %                 | 9.5               | 9.9                | 10.3               | 10.8               |
| Compressive strength | ISO 844     | MPa               | 1.1               | 2.5                | 4.3                | 7.1                |
| Compressive modulus  | ISO 844     | MPa               | 48                | 83                 | 124                | 180                |
| Shear strength       | ASTM C 273  | MPa               | 1.3               | 2.3                | 3.5                | 5.2                |
| Shear modulus        | ASTM C 273  | MPa               | 28                | 50                 | 75                 | 109                |
| Maximum shear strain | ASTM C 273  | %                 | 7.2               | 7.2                | 7.2                | 7.2                |

Technical data values presented above are typical for nominal density, subject to normal manufacturing variations.

All ROHACELL® products are closed-cell rigid foams based on polymethacrylimide (PMI) chemistry and contain no CFC's.

### Properties of ROHACELL® RIMA

| Properties           | Unit              | ROHACELL® 51 RIMA | ROHACELL® 71 RIMA | ROHACELL® 110 RIMA | Standard    |
|----------------------|-------------------|-------------------|-------------------|--------------------|-------------|
| Density              | kg/m <sup>3</sup> | 52                | 75                | 110                | ISO 845     |
|                      | lbs./cu.ft.       | 3.25              | 4.68              | 6.87               | ASTM D 1622 |
| Compressive strength | MPa               | 0.8               | 1.7               | 3.6                | ISO 844     |
|                      | psi               | 116               | 246               | 522                | ASTM D 1621 |
| Tensile strength     | MPa               | 1.6               | 2.2               | 3.7                | ISO 527-2   |
|                      | psi               | 232               | 319               | 536                | ASTM D 638  |
| Shear strength       | MPa               | 0.8               | 1.3               | 2.4                | DIN 53294   |
|                      | psi               | 116               | 188               | 348                | ASTM C 273  |
| Elastic modulus      | MPa               | 75                | 105               | 180                | ISO 527-2   |
|                      | psi               | 10,875            | 15,225            | 26,100             | ASTM D 638  |
| Shear modulus        | MPa               | 24                | 42                | 70                 | DIN 53294   |
|                      | psi               | 3,480             | 6,090             | 10,170             | ASTM C 273  |
| Strain at break      | %                 | 7                 | 7                 | 7                  | ISO 527-2   |
|                      |                   |                   |                   |                    | ASTM D 638  |

Technical data of our products are typical values for the nominal density.

### C. CFRP-foam stud testing samples naming and construction

| CFRP layup              | Foam core | Sample 1          | Sample 2          | Sample 3          |
|-------------------------|-----------|-------------------|-------------------|-------------------|
| [0/30/60] <sub>2s</sub> | RIMA 110  | <i>RIMA110/01</i> | <i>RIMA110/02</i> | <i>RIMA110/03</i> |
| [0/30/60] <sub>2s</sub> | HERO 110  | <i>HERO110/01</i> | <i>HERO110/02</i> | <i>HERO110/03</i> |
| [0/30/60] <sub>2s</sub> | HERO 200  | <i>HERO200/01</i> | <i>HERO200/02</i> | <i>HERO200/03</i> |
| [0/30/60] <sub>3s</sub> | HERO 110  | <i>HERO110/04</i> | <i>HERO110/05</i> | <i>HERO110/06</i> |
| [0/30/60] <sub>3s</sub> | HERO 200  | <i>HERO200/04</i> | <i>HERO200/05</i> | <i>HERO200/06</i> |

### D. Unidirectional CFRP data sheet

#### Mechanical properties

Material: MTM28-1/T700-36% RW  
 Cure cycle: 1 hour at 120°C (248°F), 6.2 bar (90 psi)  
 Test conditions: Room temperature, dry

| Test                                  | Test method     | Units     | Results      |
|---------------------------------------|-----------------|-----------|--------------|
| 0° Tensile strength                   | ASTM D3039      | MPa (ksi) | 2735 (397.0) |
| 0° Tensile modulus                    |                 | GPa (msi) | 127.0 (18.4) |
| 90° Tensile strength                  |                 | MPa (ksi) | 55.4 (8.04)  |
| 90° Tensile modulus                   |                 | GPa (msi) | 8.40 (1.22)  |
| 0° Compressive strength               | ASTM D695 (MOD) | MPa (ksi) | 1309 (190.0) |
| 0° Compressive modulus                |                 | GPa (msi) | 116.0 (16.8) |
| ±45 In-plane shear strength (IPSS)    | ASTM D3518      | MPa (ksi) | 127.0 (18.4) |
| ±45 In-plane shear modulus (IPSM)     |                 | GPa (msi) | 3.69 (0.54)  |
| 0° Flexural strength                  | CRAG 200        | MPa (ksi) | 1782 (258.0) |
| 0° Flexural modulus                   |                 | GPa (msi) | 117.0 (17.0) |
| 0° Interlaminar shear strength (ILSS) | ASTM D2344      | MPa (ksi) | 87.0 (12.6)  |

Data normalised to 60%Vf except for ILSS and IPSS & IPSM.

## 11. References

- Chuck Edmondson. 2011. *Fast Car Physics* p106
- Society of Automotive Engineers. 2016. *FSAE 2016 Rules*
- McLaren Racing Limited. [no date]. *Formula One Race Strategy*
- Baker et al. 2015. *Automotive Design EN4101 – Chassis Team Final Report*
- Di Marino, L. P. 2016. *Investigation into the Manufacturing and Structure of a Composite Aerofoil for a Formula Student Vehicle*
- Stengel, R. [no date], *Spacecraft Attitude Dynamics*
- Ohio State University, [no date], *Rolling, Torque and Angular Momentum*
- Uyttersprot, B. 2015. *Analysis of a carbon fibre rim*
- Giber. 2010. *Design of a carbon fiber wheel*
- Ressa, A. 2013. *Development of a carbon fiber wheel rim*
- Rohan, C. D. 2015, *Design and Analysis of a Composite Wheel Rim*
- Racecar Engineering. 2014. *FS\_2014\_Digimag Web*
- AMZFormulaStudent. 2014. *Grimsel – Virtual Assembly*[Online]. Available at:  
<https://www.youtube.com/watch?v=T2Dql2gGfk0> [accessed 10 November 2015]
- Smith, N. 2004, *Understanding Parameters influencing Tyre modeling*
- Aronsson, A. 2005, *Design, Modeling and Drafting of Composite Structures*
- TU Fast team. 2015. Conversation to members of the team at Formula Student UK 11 June 2015
- Sammons G. 2015. Email to S. Buckingham 08 October 2015
- Cardiff Racing. 2015. *September Newsletter*
- The Engineering Toolbox [web page]. *Coefficients of Linear Thermal Expansion*. Available at  
[http://www.engineeringtoolbox.com/linear-expansion-coefficients-d\\_95.html](http://www.engineeringtoolbox.com/linear-expansion-coefficients-d_95.html) visited on 22 November 2015
- Marques A. et al. 2007. *Delamination Analysis of Carbon Fiber Reinforced Laminates*
- Davis, M. *Best Practice in Adhesive Bonding*. Presented to the FAA

ASM Aerospace Specification Metals Inc. *Aluminium 6061-T6 Properties*. Available at <http://asm.matweb.com/search/SpecificMaterial.asp?bassnum=MA6061t6> Visited on 2 April 2016

Bogert P. et al. 2006. *Comparison of Damage Path Predictions for Composite Laminates by Explicit and Standard Finite Element Analysis Tools*

Svärd L. 2012. *Composites failure modeling and optimization of a spring orthosis*

Vallons K. et al. [no date]. *Fibre orientation effects on the tensile properties of biaxial carbon/epoxy ncf composites*

Kolios A. et al. 2012. *Evaluation of the Reliability Performance of Failure Criteria for Composite Structures*

Sakamoto S. et al. [no date]. *Precision drilling of CFRP (carbon fiber reinforced plastics) with coated tools*